SECURITY MARKING

The classified or limited status of this report applies to each page, unless otherwise marked.
Separate page printouts MUST be marked accordingly.

THIS DOCUMENT CONTAINS INFORMATION AFFECTING THE NATIONAL DEFENSE OF THE UNITED STATES WITHIN THE MEANING OF THE ESPIONAGE LAWS, TITLE 18, U.S.C., SECTIONS 793 AND 794. THE TRANSMISSION OR THE REVELATION OF ITS CONTENTS IN ANY MANNER TO AN UNAUTHORIZED PERSON IS PROHIBITED BY LAW.

NOTICE: When government or other drawings, specifications or other data are used for any purpose other than in connection with a definitely related government procurement operation, the U. S. Government thereby incurs no responsibility, nor any obligation whatsoever; and the fact that the Government may have formulated, furnished, or in any way supplied the said drawings, specifications, or other data is not to be regarded by implication or otherwise as in any manner licensing the holder or any other person or corporation, or conveying any rights or permission to manufacture, use or sell any patented invention that may in any way be related thereto.

COPY NO. 38

TECHNICAL MEMORANDUM 1493

SUPERSONIC FLOW ABOUT RIGHT CIRCULAR CONES AT ZERO YAW IN AIR AT CHEMICAL EQUILIBRIUM. PART I. CORRELATION OF FLOW PROPERTIES

HENRY E. HUDGINS, JR.

AUGUST 1965

AMCMS CODE 5016.11.844

PICATINNY ARSENAL
DOVER, NEW JERSEY

The findings in this report are not to be construed as an official Department of the Army position, unless so designated by other authorized documents.

DISPOSITION

Destroy this report when it is no longer needed. Do not return.

DDC AVAILABILITY NOTICE

Qualified requesters may obtain copies of this report from DDC.

Technical Memorandum 1493

SUPERSONIC FLOW ABOUT RIGHT CIRCULAR CONES AT ZERO YAW IN AIR AT CHEMICAL EQUILIBRIUM, PART I. CORRELATION OF FLOW PROPERTIES

by

Henry E. Hudgins, Jr.

August 1965

Reviewed by: 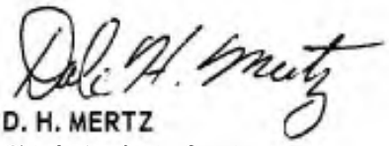

D. H. MERTZ
Chief, Analysis Section

Reviewed by: 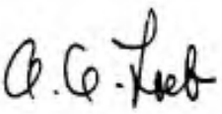

A. A. LOEB
Chief, Aeroballistics Branch

Approved by: 

W. R. BENSON
Chief, Engineering Sciences Laboratory

Feltman Research Laboratories
Picatinny Arsenal
Dover, New Jersey

ACKNOWLEDGMENT

The author wishes to express his gratitude to Dr. M. Visich of the General Applied Sciences Laboratories for his comments and contributions, and in particular for pointing out the existence and applicability of the analyses of Trimpi and Jones, and Bertram and Cook. He also wishes to thank Mr. E. Lieberman of the General Applied Sciences Laboratories, who wrote not only the program which calculated the original data, but also other programs to check the correlation formulas in this report, and who made other valuable contributions. Mr. H. Geffner of Picatinny Arsenal deserves credit for his many calculations in reducing the volumes of cone data to the forms needed for this correlation study.

TABLE OF CONTENTS

TABLE OF CONTENTS (cont)

TABLE OF CONTENTS (cont)

SUMMARY

This report (Part I) presents, in the form of correlation plots and formulas, the data tabulated in Parts II and III. This data is for the inviscid flow properties of right circular cones at zero yaw in air at chemical equilibrium. The flow properties at the cone surface or just behind the shock may be obtained directly from the correlations of this report. Methods for calculating the properties within the shock layer based on these correlations are indicated.

The range for which accurate correlations of all parameters have been found is from the region of ideal gas behavior to free stream Mach numbers up to 40 and semi-cone angles up to 40°. Some correlations are valid at least as far as semi-cone angles of 50°, the limit of the data. These results apply only to attached shocks.

TABLE OF SYMBOLS

a	local velocity of sound, ft-sec^{-1}
H	geometric altitude, ft
h	enthalpy, ft^2-sec^{-2}
K_t	2 × (stagnation enthalpy), ft^2-sec^{-2}
K_c	hypersonic similarity parameter, $M_\infty \sin \eta_c$
M	Mach number
p	pressure, lb-ft^{-2}
p_{atm}	pressure, atmospheres
R	gas constant, 1716 ft^2-sec^{-2}-R^{-1}
S	entropy, ft^2-sec^{-2}-R^{-1}
S/R	nondimensional entropy
T	temperature, degrees Kelvin or Rankine as required
u,v	velocity components, in body system, ft-sec^{-1}
W	total velocity, ft-sec^{-1}

Z	compressibility factor
γ	isentropic exponent
$\bar{\gamma}$	average value of γ in shock layer
γ_e	effective γ of Trimpi and Jones
η	ray angle in conical flow, radians
ρ	density, slug-ft^{-3}
θ	flow angle, radians

SUBSCRIPTS

∞	free stream conditions
c	at cone surface
r	component tangent to ray
s	immediately behind shock
t	component normal to ray

HISTORICAL BACKGROUND[1]

In 1929, Busemann presented a solution to the problem of determining the flow field around a right circular cone at zero angle of attack at supersonic Mach numbers in a perfect gas (Ref 1). Busemann's solution was carried out in the hodograph plane using a finite difference scheme, and the results were presented in the form of the "apple curves" of Reference 2. Taylor and Maccoll presented a solution to the same problem by integrating the conical flow equations in the physical plane (Ref 3).

With the advent of high speed computing machines, tabulated solutions of conical flow fields were published in the literature. Kopal integrated the conical flow equations using the Taylor-Maccoll solution and tabulated the resulting velocity components for $\gamma = 1.405$ (Ref 4). A major limitation of the Kopal tables is that for a given cone angle, solutions were presented

[1]This summary contributed by Dr. M. Visich.

for various values of the velocity at the surface of the cone. This resulted in conical flow solutions at discrete nonintegral values of the free-stream Mach number. Sims recomputed the conical flow fields for $\gamma = 1.400$ and a constant series of free-stream Mach numbers between 1.5 and 20 (Ref 5). The results are tabulated for a minimum semi-cone angle of 2.5 degrees to a maximum semi-cone angle of 30 degrees in 2.5-degree increments. In addition the results were tabulated for the minimum free-stream Mach number for which the conical flow field was completely supersonic. Bertram correlated the ideal air cone flow properties in terms of the hypersonic similarity parameter for free-stream Mach numbers from that for shock detachment to that approaching infinity and for semi-cone angles up to 50 degrees (Ref 6).

For reentry vehicles with conical forebodies entering the Earth's atmosphere at hypersonic Mach numbers, real gas effects must be considered in determining the conical flow variables. Feldman (Ref 7) and Romig (Ref 8) both solved the Taylor-Maccoll conical flow equations, with real gas effects included for a fixed free-stream temperature, over a range of free-stream static pressures and Mach numbers. Feldman's results assume a free-stream temperature of 392°R, while Romig's results assume a free-stream temperature of 491.7°R. A correlation of the conical flow parameters of the Feldman and Romig results is presented in Reference 9. More recently, Newman applied the Dorodnitsyn integral method to obtain an approximate algebraic solution for the equilibrium flow field around right circular cones (Ref 10). The calculations were performed at the same free-stream Mach number, pressure, and temperature conditions as the Romig calculations.

Recently, a flow field computer program was developed to determine the real gas flow field about bodies in hypersonic flight (Ref 11). This computer program uses a conical flow field subroutine to initiate the calculations around pointed axisymmetric bodies with attached shock waves. The subroutine is applicable to the computation of the supersonic flow about axisymmetric cones in equilibrium air and was used to compute the tabulated data of Reference 12.

INTRODUCTION

The availability of the conical flow computer program at Picatinny Arsenal and the obvious need for real gas cone tables over a wider range of the conditions actually existing in the Earth's atmosphere resulted in the preparation of the tabulated data for cones at zero angle of attack in equilibrium air published in Reference 12.

This report, Part I of Picatinny Arsenal Technical Memorandum 1493, analyzes the data contained in Parts II and III. The first section of this report outlines the methods used to solve for the conical flow properties in equilibrium air. The second section presents the general trends of the flow properties with the hypersonic similarity parameter, $M_\infty \sin \eta_c$.[1] The third section presents a correlation of pressures and enthalpies at the shock and at the cone surface. This makes it possible to determine the velocities for use in Busemann's hodograph technique of calculating the flow properties within the shock layer of supersonic cones, beginning at the body. The fourth section is a correlation of the flow properties based on a correlation of $M_\infty \sin \eta_s$ with K_c and the effective gamma, γ_e, of Trimpi and Jones in Reference 13. This data may also be used to calculate flow properties in the shock layer beginning at the shock and using the hodograph technique.

DISCUSSION

Method of Solution

Consider the flow around a right circular cone at zero angle of attack with an attached shock wave (Fig 1, p 30). Since the flow field around the cone is both conical and axisymmetric, all derivatives with respect to r and θ are zero. The governing equations of motion are:

The momentum equation in the η direction

$$v_t \frac{dv_t}{d\eta} + v_r v_t = -\frac{1}{\rho} \frac{dp}{d\eta} \tag{1}$$

[1] $M_\infty \sin \eta_c$ will be replaced by K_c throughout the remainder of this report.

The momentum equation in the r direction

$$v_t = \frac{dv_r}{d\eta} \tag{2}$$

The continuity equation

$$2\rho v_r \sin \eta + \frac{d}{d\eta}(\rho v_t \sin \eta) = 0 \tag{3}$$

In the isentropic conical flow field the speed of sound is given by:

$$a^2 = \left(\frac{\partial p}{\partial \rho}\right)_c = \frac{dp}{d\rho} \tag{4}$$

Substituting equation 4 into equation 3 gives

$$2v_r + v_t \cot \eta + \frac{dv_t}{d\eta} + \frac{v_t}{\rho a^2}\frac{dp}{d\eta} = 0 \tag{5}$$

Solving equations 5 and 1 for $\frac{dp}{d\eta}$ and $\frac{dv_t}{d\eta}$:

$$\frac{dp}{d\eta} = -\rho v_t\left(\frac{a^2}{v_t^2 - a^2}\right)(v_r + v_t \cot \eta) \tag{6}$$

$$\frac{dv_t}{d\eta} = \left(\frac{a^2}{v_t^2 - a^2}\right)\left(2v_r + v_t \cot \eta - \frac{v_r v_t^2}{a^2}\right) \tag{7}$$

The differential equations are integrated by writing them in finite difference form and using a Taylor series expansion for the dependent variables of the form

$$p_n = p_{n-1} + \left(\frac{dp}{d\eta}\right)_{n-1} \Delta\eta \tag{8}$$

$$v_{t_n} = v_{t_{n-1}} + \left(\frac{dv_t}{d\eta}\right)_{n-1} \Delta\eta \tag{9}$$

$$v_{r_n} = v_{r_{n-1}} + v_{t_{n-1}}\Delta\eta + \left(\frac{dv_t}{d\eta}\right)_{n-1} \tfrac{1}{2}(\Delta\eta)^2 \tag{10}$$

The boundary conditions for the conical field are that at $\eta = \eta_c$, $v_t = 0$ and that at $\eta = \eta_s$ the flow behind the conical shock wave satisfies the shock wave equations requiring conservation of:

mass

$$\rho_\infty W_\infty \sin \eta_s = \rho_s W_s \sin (\eta_s - \theta_s) \tag{11}$$

normal momentum

$$p_\infty + \rho_\infty (W_\infty \sin \eta_s)^2 = p_s + \rho_s W_s^2 \sin^2(\eta_s - \theta_s) \tag{12}$$

tangential momentum

$$\rho_\infty W_\infty^2 \sin \eta_s \cos \eta_s = \rho_s W_s^2 \sin(\eta_s - \theta_s) \cos (\eta_s - \theta_s) \tag{13}$$

and energy

$$\tfrac{1}{2} W_\infty^2 + h_\infty = \tfrac{1}{2} W_s^2 + h_s = \tfrac{1}{2} K_1 \tag{14}$$

together with the requirement that:

$$\Delta S = S_s - S_\infty \geq 0 \tag{15}$$

In order to determine the flow field between the shock wave and the surface of the cone, the conical flow field is assumed to be in chemical equilibrium. For a given free-stream Mach number and altitude, the shock wave angle is assumed. Ideal gas values are used for the first guess. The flow conditions immediately behind the shock wave are then determined using the thermodynamic properties of air either from the vibrational excitation analysis of Reference 11 or from the AEDC numerical fits of Reference 14. (The loci of points which define the lower bounds of validity of the AEDC fits correspond to a compressibility factor, Z, of unity. The effect of crossing these bounds is to cause a discontinuity in the gradients of certain parameters. The most noticeable "jump" occurs in the speed of sound and hence in the value of γ. A smaller jump occurs in the other flow properties while crossing these bounds.)

The finite difference equations were solved on the IBM 7090 computer at Picatinny Arsenal. Assuming the shock wave angle, these equations were solved using 100 steps from the assumed shock wave to the required cone surface. If the boundary condition of $v_t = 0$ at $\eta = \eta_c$ was not satisfied, an iteration scheme based on the Newton-Raphson technique was used until the correct value of the shock wave was determined to within at least ±0.001 degree. After converging to the correct shock angle, the thermodynamic properties of the gas were tabulated at every tenth integration step. Numerical results are tabulated in Reference 12 for the following range of parameters:

Altitude:	sea level to 200,000 ft
Free-stream Mach number:	3 to 40
Semi-cone angle:	2.5° to 50°

With the values of p, S/R, v_r, and v_t known, ρ, θ, μ, and γ were calculated.

In the following section a discussion of the results of the numerical calculation will be presented as well as a correlation of those results.

General Trends of Flow Properties

The first group of graphs present the general trends of various flow parameters with the hypersonic similarity parameter, K_c, and altitude. The equilibrium results are compared with the ideal results from References 5 and 6.

It was determined from earlier experimental computer runs, prior to preparing Parts II and III of this report, that γ (defined as the isentropic exponent) varied less than 0.1% within the shock layer. For an example, see Table 1 (p 20). Therefore, only an average gamma, $\bar{\gamma}$, was printed as output. In Figure 2 (p 31) the trend of $\bar{\gamma}$ with K_c and altitude is shown. The detailed information is given in Table 2 (p 21).

The pressure at the cone surface in the form of p_c/p_∞ is presented in Figure 3 (p 32). Note that the equilibrium air curve is indistinguishable graphically from the ideal air curve for all altitudes. Comparison with the ideal air results of Sims (Ref 5) shows agreement to within 2%. Since the pressure forces do not vary significantly from the ideal case, the values of C_{N_α} in Reference 6 are valid for equilibrium air as well. Pressure correlation at the surface and behind the shock is discussed in more detail later in this report.

The ratio of cone surface density to free-stream density is shown in Figure 4 (p 33). This is clearly a function of altitude and diverges rapidly from the ideal air case, which becomes asymptotic to $\left(\frac{\gamma_\infty + 1}{\gamma_\infty - 1}\right)\left(\frac{\gamma_\infty + 7}{8}\right)^{1/\gamma_\infty}$ as M_∞ approaches infinity. Ideal gas calculations for density are valid up to a value of 3 for K_c, based on agreement to within 5% with the equilibrium calculations.

Figure 5 (p 34) presents the ratio of surface temperature to free-stream temperature versus the hypersonic similarity parameter. Again the divergence from the ideal gas model is marked at the higher values of K_c. As expected, equilibrium gas temperatures are lower due to the absorption of energy by ionization and dissociation. Ideal gas temperature calculations are useful up to a value of 4 for the hypersonic similarity parameter, again based on agreement within 5%.

The entropy increase across the shock is nondimensionalized by the gas constant and plotted in Figure 6 (p 35). Since the shock layer in conical flow is isentropic, the values at the body are the same as at the shock. The increase in equilibrium air entropy is seen to be greater than that for ideal air and is also a function of altitude. At values of K_c less than 5, the difference between the ideal and equilibrium air calculations is 5% or less. For K_c greater than approximately 5 the entropy increase across the shock can be correlated by an equation of the form (from a private communication with M. Visich (Ref 15):

$$\log_{10}\left(\frac{\Delta S}{R}\right) = A \log_{10}(K_c) - B \qquad (16)$$

where A and B are functions of altitude. The values of A and B are listed in Table 3 (p 22). Also given in Table 3 is the value of K_c for which the above equation has an error of 1% or less.

Figure 7 is made more complicated by the fact that the ratio of surface to free-stream Mach number is not independent of cone angle when plotted versus K_c. Thus, ideal values are shown in Figure 7A (p 36), and equilibrium values for sea level in 7B (p 37) and for 200,000 feet in 7C (p 38). Real air surface Mach numbers are increased, for a given value of K_c, over the ideal surface during the trade-off on lowering $\bar{\gamma}$ and rising temperatures. Also the higher altitudes result in higher ratios of M_c/M_∞ for a given value of the hypersonic similarity parameter.

The preceding curves may also be used to determine the accuracy of using ideal gas calculations for a real gas. It can be seen that the acceptable limits vary with the particular parameter of concern and with the desired accuracy.

Some crossing of the curves for different altitudes can be seen for the temperature and density ratios. These crossings occur through the range of K_c during which transition within the computer program takes place from the vibrational excitation analysis to the equilibrium air properties of the AEDC fits. This transition boundary in terms of the conical analysis is illustrated in Figure 8 (p 39). The discontinuities are more pronounced at the higher altitudes for two reasons: one, the AEDC fits are poorest in the low pressure regions; two, the actual degree of ionization and dissociation at the transition is significant.

Velocities at the cone surface and just behind the shock may be obtained from the enthalpy curves given later by use of the relation:

$$W = (K_t - 2h)^{1/2} \tag{17}$$

Figures 9, 10, and 11 (pp 40-42) present the ratio of surface properties to properties just behind the shock for pressure, density, and temperature, respectively. The discontinuities for $6 < K_c < 8$ (at transition) are more obvious here than in the previous figures. Figures 9, 10, and 11 indicate that the real gas effect is to reduce the pressure, density, and temperature differences through the shock layer compared to the ideal air analysis. The ideal air asymptotes as M_∞ approaches infinity are:

$$\frac{p_c}{p_s} = \left(\frac{\gamma_\infty + 1}{8}\right), \quad \frac{\rho_c}{\rho_s} = \left(\frac{\gamma_\infty + 1}{8}\right)^{1/\gamma_\infty},$$

$$\text{and } \frac{T_c}{T_s} = \left(\frac{\gamma_\infty + 1}{8}\right)^{\frac{\gamma_\infty - 1}{\gamma_\infty}}$$

The purpose of this equilibrium air cone study was to extend the scope of cone data, not to duplicate the ideal air data available. Therefore, coverage at the lower values of K_c is incomplete. The ideal gas correlation curves of Reference 16 or the tabulated data of Reference 14 should be

used when this report indicates that the air may be treated as ideal and does not include the desired case.

Pressure and Enthalpy Correlations

This portion of the report deals with the correlation of pressure and enthalpy just behind the shock and at the cone surface with the hypersonic similarity parameter, K_c. The formulas presented here are the results of least square fits to the data in Reference 12. That data was reduced to the form of K_c versus the pressure and enthalpy ratios for sea level and 200,000 feet altitudes. These were plotted versus K_c with 100 data points for each parameter at each altitude. The plots revealed that a correlation with K_c alone was possible as the pressures and enthalpies were virtually independent of altitude, or pressure. Forty-five points were used from each altitude, for a total of 90, in the least squares curve fitting program. These points were selected by using K_c values of approximately 1.5, 2, 3, 4, 5, 6, 7, 9, 11, 13, 15, 17, 20, 23, and 27. Each value of K_c was represented by three combinations of Mach number and cone semi-angle for each of the two altitudes. For a given value of K_c and altitude these combinations were the median values of Mach number and angle, the largest angle and lowest Mach number, and the highest Mach number and smallest angle available from the data.

The accuracies quoted for equations 18 through 21a are based on the deviations of the points which were fitted from the equation prescribed by the least squares fit.

The ratio of the pressure immediately behind the shock to the ambient pressure can be correlated by the following formulas:

$$\frac{p_s}{p_\infty} \quad 1.3928\,(K_c)^{2.0023} + 1.0181 \qquad (18)$$

or

$$\frac{p_s}{p_\infty} \quad 1.5961 - 0.3779\,(K_c) + 1.4229\,(K_c)^2 \qquad (18a)$$

The accuracy of equation 18 for predicting the pressure ratios at the shock over the range of parameters for which the conical flow solutions were fitted to the reduced data of Reference 12 is 1.5%. The accuracy is better than 0.5% for values of K_c over 8. Equation 18a is accurate to within 3% over the range, and is accurate to better than 1% for values of K_c greater than 6.

The ratio of cone surface pressure to ambient pressure may be correlated by the following functions of K_c:

$$\frac{P_c}{P_\infty} = 1.4932\,(K_c)^{1.9854} + 1.3017 \tag{19}$$

or

$$\frac{P_c}{P_\infty} = 1.6584 - 0.1399\,(K_c) + 1.4410\,(K_c)^2 \tag{19a}$$

Equation 19 represents, with an accuracy of better than 1.5%, the pressure ratio at the body over the range of parameters for which conical flow data was fitted. For values of K_c over 6, the error is less than 1%. The accuracy of equation 19a is better than 2.5% over the range and is better than 1% for values of K_c in excess of 8.

The ratio of the enthalpy just behind the shock to the free-stream enthalpy can be correlated by the following formulas:

$$\frac{h_s}{h_\infty} = 1.0794 + 0.2450\,(K_c)^{1.9506} \tag{20}$$

or

$$\frac{h_s}{h_\infty} = 0.9451 + 0.1305\,K_c + 0.2092\,K_c^2 \tag{20a}$$

The accuracy of Equation 20 for predicting the enthalpy ratio at the shock for the range of parameters for which conical flow data was fitted is better than 2%. The accuracy seems to be independent of (K_c). Equation 20a has a maximum error of 5% over the range and is accurate to within 2% for K_c over 10.

The ratio of the enthalpy at the cone surface to the free-stream enthalpy may be correlated with the following functions of K_c:

$$\frac{h_c}{h_\infty} = 1.2396\,(K_c)^{1.9668} + 1.1193 \tag{21}$$

or

$$\frac{h_c}{h_\infty} = 1.0023 + 0.1280\,K_c + 0.2106\,K_c^2 \tag{21a}$$

Equation 21 predicts the enthalpy ratio to within 3% over the range of parameters for which conical flow data was fitted. For values of K_c over 6 it is accurate to within 2%. The accuracy of Equation 21a over the range is better than 1% and is better than 2% for K_c greater than 10.

The correlation of enthalpy with K_c makes it possible to determine the variation of velocity with K_c by means of Equation 17. The error in a velocity which is calculated from an enthalpy is less than one-half the error in the enthalpy. Thus, excellent velocity accuracy may be achieved.

Plots of the preceding equations are shown in Figures 12 through 15 (pp 43-46). Alternative algebraic forms cannot be distinguished graphically.

Once the velocities at the body and shock are known for a given cone and flight condition, and the value of $\bar{y}$ within the shock layer is known from Figure 2 (p 31) or Table 2 (p 21), it is possible then to calculate the flow within the shock layer. This is done by means of the hodograph method of Busemann's which is described in Chapter 12 of Reference 17. The calculation is initiated at the cone surface with the known values of η_c, W_c, and $\bar{y}$ and is carried in steps toward the shock. The shock is defined by $W = W_s$, and η_s is an output of the calculation.

Effective Gamma Correlation

In this part of the report we are concerned with the correlation of flow properties behind the shock based upon the effective gamma definition of Reference 13 and the results of References 3 and 13. While these references should be consulted for details, an outline will be given here of the correlations at the shock for density, velocity, pressure, enthalpy, and flow deflection angle.

The basic definitions are:

$$M_N^2 = (M_\infty \sin \eta_s)^2 \qquad (22)$$

$$\gamma_e = 2\left(\frac{M_N^{-2} - 1}{\frac{P_\infty}{P_s} - 1}\right) - 1 \qquad (23)$$

Conversely,

$$\frac{\rho_s}{\rho_\infty} \quad \frac{M_N^2(\gamma_e + 1)}{M_N^2(\gamma_e - 1) + 2} \tag{23a}$$

From Reference 13

$$\frac{W_s}{W_\infty} \quad \frac{1}{\cos \theta_s} \left[1 + \left(\frac{\rho_\infty}{\rho_s} - 1 \right) \sin^2 \eta_s \right] \tag{24}$$

and in Reference 18, combining the momentum and continuity equations with the definition of γ_e yields:

$$\frac{P_s}{P_\infty} \quad 1 + \left(\frac{2\gamma_\infty}{\gamma_e + 1} \right) (M_N^2 - 1) \tag{25}$$

Combining the energy and mass flow equations in Reference 18 results in.

$$\frac{h_s}{h_\infty} \quad \left(\frac{\gamma_\infty - 1}{2} \right) M_N^2 \left[1 - \left(\frac{\rho_\infty}{\rho_s} \right)^2 \right] \tag{26}$$

An analytical approach to calculating θ_s for conical flow may be made by using the oblique flow analysis of Reference 13. From continuity and the definition of γ_e:

$$\frac{\tan (\eta_s - \theta_s)}{\tan \eta_s} \quad \frac{\left(\frac{1}{M_N^2} - 1 \right)}{\left(\frac{\gamma_e + 1}{2} \right)} + 1 \tag{27}$$

with η_s corresponding to the $K - \pi/2$ of Reference 13. Rewriting equation 27 results in:

$$\frac{-\cot \eta_s}{\tan \theta_s} \quad 1 + \left[\frac{\left(\frac{\gamma_e + 1}{2} \right)}{\left(\frac{1}{M_\infty} \right)^2 - \sin^2 \eta_s} \right] \tag{28}$$

which can be simplified to:

$$\tan \theta_s \quad \frac{\cot \eta_s}{\left[\frac{(\gamma_e + 1)M_\infty^2}{2(M_N^2 - 1)}\right] - 1} \tag{28a}$$

The determination of the entropy in the shock layer can be accomplished by the use of equation 16, which correlates $\Delta S/R$ with K_c and altitude, or by using Figure 6 (p 35), which presents the data graphically.

Or as η_s, ρ_s, p_s are determined, entropy as well as such variables as temperature, speed of sound, and the isentropic exponent may now be determined with the use of tables or charts of the thermodynamic properties of air. However, the flow deflection and shock angle must be known, as well as the cone angle and ambient pressure.

Equations 24, 25, 26, 27, 28, and 28a are exact if γ_e is calculated from the actual density ratio across the shock, and if the actual shock angle is known.

The values of γ_e for a number of altitudes were calculated from the data in Reference 12 and are shown in Table 4 (p 23). Trends are indicated in Figure 16 (p 47). The correlation was quite good. The use of this correlated data introduces some small degree of approximation into the equations, but as shown in Table 5 (p 24) the prediction of properties is excellent.

Although excellent analytical prediction of the flow deflection for a known shock angle is available, it may be of interest to have an empirical correlation with the hypersonic similarity parameter as well. It was found that such an equation can be formed (see also Figure 17, p 48) if altitude effects are allowed for by a pressure term. This equation, using pressure in psf, is:

$$M_\infty \sin \theta_s = (.97245 - .001863 \log_{10} p_\infty) K_c - (.32908 - .000243 \log_{10} p_\infty) \tag{29}$$

Clearly, this equation is not a good approximation for η_c near 0° since $\sin \theta_s$ must approach zero at this point. Nor is it valid for values for η_c greater than the shock detachment angle. Within these limitations, equation 30 represents the flow deflection angle to better than 5%.

It will be noted, however, that the shock angle is still required to calculate all of the properties at the shock. Usually the cone angle is known, but the shock angle is not. Therefore, a correlation between the two angles was sought and found.

The variation of $M_\infty(\sin \eta_s - \sin \eta_c)$ with K_c and altitude is presented in Figure 18 (p 49). The data points for cone angles greater than 40° begin to depart significantly from the general trend for a given altitude. Therefore, the following correlations only apply to $\eta_c \leq 40°$.

As a check with Romig's correlation (Ref 19) of shock-angle and cone angle, a linear least squares fit was made to each altitude of Figure 18. Table 6 (p 29) compares the coefficients of the fit to this data with those computed with Romig's equation, based on $M_\infty \sin \eta_s = A_0 + A_1(K_c)$ for K_c greater than 6, where for Romig:

$$A_0 = 0.39 - 0.01 \log_{10} p_{atm} \tag{30}$$

$$A_1 = 1.03 + 0.005 \log_{10} p_{atm} \tag{30a}$$

The function $M_\infty(\sin \eta_s - \sin \eta_c) = A_0 + (A_1 - 1)K_c$ is plotted in Figure 19 (p 50). This illustrates that the coefficients of this study are low at the lower altitudes and high at the upper altitudes when compared with Romig. A weighted average for best results over the entire range, as done by Romig, would probably give results even closer to Romig's. However, this approach was not followed up because of a better correlation discussed later.

It has been pointed out that an accurate means of predicting the shock angle, when the cone angle is known, is required to make the equations truly useful. Bertram in Reference 18 writes an approximate equation for $M_\infty \sin \eta_s$ in an extended hypersonic similarity form which requires θ_s. The empirical correlation of θ_s with K_c of this report, equation 30, and Figure 17 (p 48), could be used to calculate $M_\infty \sin \eta_s$. Another, and simpler, approach is to use the quite accurate correlation of p_s / p_∞ with K_c of equation 18.

Equation 18 can be converted to

$$\left(\frac{p_s}{p_\infty}\right) - 1 = \gamma_\infty (K_c)^2 \tag{31}$$

by the rounding off to the first decimal place of the constants in the curve fit, since $\gamma_\infty = 1.4$ for air. When this result is substituted into the correlation of equation 10 we find that:

$$M_\infty \sin \eta_s \doteq \left[\left(\frac{\gamma_e + 1}{2}\right)(K_c)^2\right]^{1/2} \tag{32}$$

In order to obtain better graphical accuracy, the ordinate of Figure 20 (p 51) is $M_\infty(\sin \eta_s - \sin \eta_c)$ and the abscissa is the quantity X, where:

$$X \equiv \left[\left(\frac{\gamma_e + 1}{2}\right)(K_c)^2 + 1\right]^{1/2} - K_c \tag{33}$$

This would be identical to $M_\infty(\sin \eta_s - \sin \eta_c)$, using equation 32, except for the one added to the K_c term. This term was found to improve the fit for low values of K_c without appreciably altering the fit at the higher values. It is basically a correction for the fact that γ_e must be initially selected by assuming that $M_\infty \sin \eta_s$ equals K_c, since γ_e is available as a function of $M_\infty \sin \eta_s$. A study of the correlation of γ_e with K_c and its accuracy in correlating this data is being made.

A least squares fit was made to the points on Figure 20 using first and second order polymonials. Since the two fits were of nearly equal accuracy in their fit to the data, the first order polynomial will be used for simplicity. The resulting equation is:

$$M_\infty(\sin \eta_s - \sin \eta_c) \doteq -0.01550 + 0.9990\,X \tag{34}$$

If the coefficient of X be made equal to one, the best fit is:

$$M_\infty(\sin \eta_s - \sin \eta_c) = -.01617 + X \tag{34a}$$

As can be seen from Figure 20, over most of the range of Mach numbers, cone angles, and altitudes, the error in $M_\infty(\sin \eta_s - \sin \eta_c)$ is less than 2.5%. For a small range of the hypersonic similarity parameter at 200,000 feet, the error reaches a maximum value of 7%. The data points of Figure 20 were calculated using values of γ_e from Reference 18. By using Figure 18 to estimate the bounding values of the ratio of $M_\infty(\sin \eta_s - \sin \eta_c)$ to

K_c, we conclude that the ratio is less than 1/5 at $K_c = 2$ and less than 1/20 at $K_c = 25$. Therefore, the error in $M_\infty \sin \eta_s$ is between 1/5 to 1/20 of that in $M_\infty (\sin \eta_s - \sin \eta_c)$ for a given value of the hypersonic similarity parameter. It can be expected for most cases that the error in shock angle will be much less than 1%, with the greater accuracy at the higher values of K_c.

Table 6 compares the computer results of the cone tables with the results of the correlation equations 23a, 24, 25, and 28a and the value of η_s calculated from equation 34a for a range of Mach numbers, cone angles, and altitudes. The cases were chosen to be a representative cross section of the data in Reference 12.

CONCLUSIONS

The conical flow properties just behind the shock and the shock-layer thickness are well determined by an effective gamma correlation for a known Mach number, cone semi-angle, and altitude. The values of γ_e are tabulated. The pressures and enthalpies and hence, velocities, are also well determined at the shock and body by correlation with the hypersonic similarity parameter.

The assumption of a constant gamma, $\bar{\gamma}$, within the shock layer is valid. The value of $\bar{\gamma}$ as a function of the hypersonic similarity parameter and altitude has been tabulated.

All the information needed to use the hodograph technique for conical flow described in Chapter 12 of Reference 17 is presented here. Enough information is available to solve for the flow in the shock layer beginning at the shock or the cone surface. The "forward" method employs the γ_e correlation, and the "backward" method uses the enthalpy correlation with K_c. These approaches make feasible the hand calculation of properties within an equilibrium conical shock layer.

An evaluation of the relative convenience and accuracy within the shock layer of these two approaches, unfortunately, cannot be included in this report. It is hoped a later report answering this question will be issued.

REFERENCES

1. Busemann, A., "Drücke auf kegelförmige Spitzen bei Bewegung und Überschallgeschwindigkeit," *ZAMM* 9, p 498, 1929

2. Busemann, A., "Conical Supersonic Flow with Axial Symmetry," *Luftfahrtforschung* 19, pp 134-144, 1942

3. Taylor, G. I., and Maccoll, J. W., "The Air Pressure on a Cone Moving at High Speeds," *Proc. Royal Soc.*, A139, 278-311, 1933

4. Kopal, Zdenek, "Tables of Supersonic Flow Around Cones," MIT Technical Report 1, 1947

5. Sims, Joseph L., "Tables for Supersonic Flow Around Right Circular Cones at Zero Angle of Attack," NASA SP-3004, 1964

6. Bertram, Mitchel H., "Correlation Graphs for Supersonic Flow Around Right Circular Cones at Zero Yaw in Air as a Perfect Gas," NASA TN-D-2058, January 1964

7. Feldman, S. R., "Hypersonic Conical Shocks for Dissociated Air in Thermodynamic Equilibrium," *Jet Propulsion*, Vol 27, No. 12, pp 1253-1255, December 1957

8. Romig, M. F., "Conical Flow Parameters for Air in Dissociation Equilibrium: Final Results," Convair Scientific Research Laboratory Research Note 14, January 1958

9. Romig, M. F., "Application of the Hypersonic Similarity Rule to Conical Flow of Dissociated Air," *AeroSpace Engineering*, Vol 18, No. 3, pp 56-59, 75, March 1959

10. Newman, P. A., "Approximate Calculation of Hypersonic Conical Flow Parameters for Air in Thermodynamic Equilibrium," NASA TN-D-2058, January 1964

11. Liebermann, E., "Computer Programs and Analysis for Flow Fields About Bodies in Hypersonic Flight-Air in Chemical Equilibrium and Frozen Flow Chemistry," GASL Technical Report 460, September 1964

12. Hudgins, Henry, "Supersonic Flow About Right Circular Cones at Zero Yaw in Air at Chemical Equilibrium," Parts II and III, Picatinny Arsenal Technical Memorandum 1493, September 1964

13. Trimpi, Robert L., and Jones, Robert A., "A Method of Solution with Tabulated Results for the Attached Oblique Shock-Wave System for Surfaces at Various Angles of Attack, Sweep, and Dihedral in an Equilibrium Real Gas Including the Atmosphere," NASA TR R-63, 1960

14. Lewis, C. H. and Burgess, E., "Empirical Equations for the Thermodynamic Properties of Air and Nitrogen to 15,000°K," AEDC TDR-63-138, July 1963

15. Visich, Marian, Private communication, April 1965

16. Ames Research Staff, "Equations, Tables, and Charts for Compressible Flow," NACA Report 1135

17. Ferri, Antonio, *Elements of Aerodynamics of Supersonic Flows*, The MacMillen Co., N. Y., 1949

18. Bertram, Mitchel H. and Cook, Barbara S., "The Correlation of Oblique Shock Parameters for Ratios of Specific Heats from 1 to 5/3 with Application to Real Gas Flows," NASA TR-R-171

19. Romig, Mary F., "Comment on Conical Shock Wave Angle," *AIAA Journal*, pp 2232-2233, December 1964

TABLE 1

Example of the variation of gamma in shock layer

Cone semi-angle = 45.0°

Mach no. = 20.0

Altitude = 200,000 ft

ETA (deg)	GAMMA
47.6666 (shock)	1.11618
47.3999	1.11618
47.1333	1.11617
46.8666	1.11616
46.5999	1.11616
46.3333	1.11615
46.0666	1.11615
45.8000	1.11614
45.5333	1.11614
45.2666	1.11614
45.0000 (body)	1.11614

TABLE 2

Average gamma in conical shock layer

K_c	Altitude in Feet (U. S. Standard Atmosphere, 1962)									
	0	25,000	36,100	65,900	80,000	100,000	125,000	155,500	172,500	200,000
1	1.40	1.40	1.40	1.40	1.40	1.40	1.40	1.40	1.40	1.40
2	1.395	1.388	1.392	1.392	1.391	1.390	1.387	1.381	1.381	1.383
4	1.318	1.328	1.334	1.335	1.333	1.331	1.327	1.321	1.321	1.325
6	1.297	1.301	1.303	1.303	1.303	1.302	1.300	1.298	1.298	1.299
7	1.280	1.288	1.297	1.297	1.296	1.260	1.160	1.129	1.124	1.122
8	1.222	1.230	1.240	1.195	1.170	1.155	1.132	1.122	1.119	1.114
9	1.200	1.195	1.195	1.165	1.158	1.141	1.134	1.140	1.140	1.128
10	1.205	1.188	1.180	1.160	1.155	1.153	1.153	1.170	1.152	1.157
11	1.225	1.200	1.182	1.175	1.175	1.200	1.187	1.210	1.185	1.175
12	1.242	1.222	1.190	1.200	1.220	1.210	1.220	1.220	1.220	1.231
13	1.225	1.225	1.226	1.220	1.225	1.220	1.205	1.185	1.185	1.185
14	1.205	1.223	1.230	1.220	1.205	1.205	1.185	1.160	1.160	1.160
16	1.188	1.193	1.198	1.188	1.180	1.167	1.153	1.136	1.135	1.132
18	1.185	1.180	1.180	1.168	1.162	1.158	1.141	1.130	1.125	1.120
20	1.190	1.178	1.175	1.163	1.156	1.150	1.143	1.137	1.131	1.122
22	1.200	1.185	1.177	1.162	1.162	1.157	1.153	1.153	1.146	1.134
24	1.204	1.194	1.186	1.176	1.174	1.170	1.165	1.165	1.160	1.150
26	1.260	1.204	1.196	1.190	1.186	1.178	1.175	1.167	1.165	1.153
27	1.270	1.209	1.200	1.195	1.193	1.188	1.177	1.238	1.238	1.200
28	1.265	1.235	1.207	1.202	1.200	1.189	1.235	1.216	1.210	1.225
29	1.250	1.265	1.225	1.207	1.230	1.220	1.230	1.205	1.197	1.210
30	1.240	1.265	1.254	1.240	1.225	1.225	1.223	1.195	1.190	1.190

TABLE 3

Correlation coefficients of $\Delta S/R$ with K_c

$\log_{10}(\Delta S/R) = A \log_{10}(K_c) - B$

Altitude (ft)	A	B	(K_c) Minimum
0	0.9839	0.1157	7.5
65,900	1.0002	0.1494	7.0
100,000	1.0567	0.1977	6.0
125,000	1.1092	0.2387	6.0
155,500	1.1710	0.2832	5.5
200,000	1.1987	0.3110	5.0

TABLE 4

Effective gamma calculated from density ratio across conical shock

$M_\infty \sin \eta_s$	Altitude in Feet (U. S. Standard Atmosphere, 1962)									
	0	25,000	36,100	65,900	80,000	100,000	125,000	155,500	172,500	200,000
1	1.40	1.40	1.40	1.40	1.40	1.40	1.40	1.40	1.40	1.40
2	1.392	1.398	1.399	1.398	1.399	1.398	1.397	1.395	1.395	1.395
3	1.378	1.387	1.392	1.391	1.392	1.390	1.387	1.384	1.383	1.383
4	1.360	1.372	1.378	1.378	1.377	1.374	1.370	1.364	1.366	1.367
6	1.324	1.335	1.347	1.346	1.342	1.341	1.339	1.332	1.325	1.330
8	1.282	1.301	1.320	1.320	1.309	1.307	1.297	1.270	1.260	1.270
10	1.251	1.266	1.275	1.269	1.263	1.253	1.237	1.200	1.200	1.204
12	1.227	1.234	1.240	1.230	1.222	1.215	1.196	1.186	1.188	1.180
13	1.223	1.224	1.231	1.219	1.213	1.208	1.194	1.185	1.186	1.183
14	1.222	1.222	1.225	1.214	1.210	1.205	1.193	1.184	1.185	1.185
15	1.220	1.221	1.221	1.213	1.209	1.201	1.192	1.179	1.175	1.178
16	1.215	1.218	1.199	1.210	1.206	1.199	1.186	1.169	1.165	1.167
18	1.203	1.209	1.211	1.201	1.195	1.181	1.171	1.153	1.150	1.152
20	1.192	1.198	1.200	1.189	1.181	1.161	1.146	1.143	1.138	1.137
22	1.184	1.186	1.188	1.175	1.170	1.161	1.146	1.133	1.130	1.127
24	1.175	1.178	1.178	1.166	1.161	1.152	1.138	1.127	1.123	1.120
26	1.170	1.173	1.171	1.159	1.155	1.145	1.130	1.128	1.123	1.118
28	1.173	1.168	1.1666	1.154	1.151	1.142	1.132	1.133	1.128	1.123
30	1.186	1.164	1.163	1.152	1.148	1.141	1.142	1.139	1.140	1.132

TABLE 5

Comparison of results of conical flow correlation formulas and cone table values

Configuration		Properties from Tables					Properties Calculated from Correlations				
η_c deg	M_∞ W_∞/a_∞	η_s deg	Rho_s ρ_s/ρ_∞	P_s p_s/p_∞	θ_s rad	V_s W_s/W_∞	η_s deg	Rho_s ρ_s/ρ_∞	P_s p_s/p_∞	θ_s rad	V_s W_s/W_∞
					ALTITUDE = 0 FEET						
3	30	39.7449	2.553	4.133	.3788	.80856	39.4353	2.553	4.133	.3788	.80865
3	40	51.6354	3.182	6.312	.5233	.66766	50.5595	3.182	6.312	.5232	.66778
10	20	22.5731	4.744	17.280	.3066	.92692	22.5384	4.744	17.281	.3065	.92692
10	30	33.2999	5.809	35.935	.4686	.84113	33.2224	5.809	35.935	.4685	.84113
10	40	44.2008	6.729	58.935	.6279	.72434	44.0301	6.729	58.935	.6279	.72634
5	20	6.1213	2.876	5.153	.0696	.99499	6.1478	2.876	5.154	.0695	.99498
20	20	21.6512	6.998	66.338	.3212	.93094	21.6297	6.998	66.338	.3212	.93094
20	30	32.1192	8.585	140.864	.4876	.84920	32.0811	8.585	140.865	.4875	.84920
20	40	42.8433	9.440	232.512	.6498	.73674	42.7656	9.440	232.510	.6498	.73674
2.5	30	3.2880	2.236	3.291	.0317	.99868	3.3071	2.236	3.291	.0316	.99868
20	30	21.2957	8.722	148.139	.3270	.93265	21.2810	8.722	148.140	.3270	.93264
30	30	31.8243	9.844	315.770	.4925	.85135	31.8003	9.844	315.768	.4924	.85135
40	30	42.3576	11.095	521.786	.6576	.74123	42.3250	11.095	521.785	.6575	.74123
2.5	40	3.0853	2.878	5.160	.0348	.99875	3.0642	2.878	5.161	.0348	.99874
20	40	21.1732	9.562	262.663	.3291	.93326	21.1645	9.562	262.663	.3290	.93325
30	40	31.5709	11.306	560.696	.4967	.85325	31.5528	11.306	560.694	.4967	.85325
40	40	42.0854	12.510	926.816	.6625	.74408	42.0454	12.510	926.814	.6624	.74407

TABLE 5 (cont)

Configuration		Properties from Tables					Properties Calculated from Correlations				
η_c deg	M_∞ W_∞/a_∞	η_s deg	Rho_s ρ_s/ρ_∞	P_s p_s/p_∞	θ_s rad	V_s W_s/W_∞	η_s deg	Rho_s ρ_s/ρ_∞	P_s p_s/p_∞	θ_s rad	V_s W_s/W_∞
					ALTITUDE = 65,900 FEET						
22.5	3	32.0020	2.015	2.782	.2578	.88780	32.0152	2.015	2.783	.2578	.88787
30	3	39.7874	2.547	4.134	.3784	.80837	39.4728	2.547	4.134	.3784	.80845
40	3	51.7637	3.163	6.316	.5219	.66674	50.6575	3.163	6.316	.5218	.66686
45	3	59.0773	3.432	7.571	.5783	.57132	56.8563	3.432	7.571	.5783	.57144
20	10	22.6517	4.626	17.276	.3054	.92660	22.6198	4.626	17.276	.3053	.92661
40	10	44.5941	6.243	58.955	.6217	.72091	44.4105	6.243	58.954	.6216	.72092
5	20	6.1280	2.864	5.153	.0695	.99498	6.1387	2.864	5.153	.0694	.99498
20	20	21.8318	6.376	66.300	.3183	.93011	21.8177	6.376	66.299	.3182	.93011
40	20	42.7075	9.862	232.495	.6521	.73803	42.6301	9.862	232.495	.6520	.73893
5	30	5.7652	3.907	10.460	.0748	.99527	5.9870	3.907	10.460	.0747	.99527
20	30	21.3338	8.484	148.106	.3263	.93246	21.3226	8.484	148.106	.3263	.93246
40	30	42.3090	11.385	521.761	.6587	.74188	44.5061	11.385	521.763	.6586	.74188
5	40	5.6190	4.674	.17881	.0770	.99541	5.6167	4.674	17.880	.0770	.99541
20	40	21.1336	9.874	262.693	.3297	.93346	21.1307	9.874	262.692	.3297	.93345
40	40	41.9271	13.449	926.728	.6651	.74565	41.8901	13.449	926.732	.6650	.74565

TABLE 5 (cont)

Configuration		Properties from Tables					Properties Calculated from Correlations				
η_c deg	M_∞ W_∞/a_∞	η_s deg	Rho_s ρ_s/ρ_∞	P_s p_s/p_∞	θ_s rad	V_s W_s/W_∞	η_s deg	Rho_s ρ_s/ρ_∞	P_s p_s/p_∞	θ_s rad	V_s W_s/W_∞
ALTITUDE = 155,500 FEET											
22.5	3	31.9938	2.015	2.782	.2578	.88783	32.0129	2.015	2.782	.2577	.88793
30	3	39.7597	2.551	4.133	.3786	.80850	39.4482	2.5510	4.1336	.3786	.80858
40	3	51.6751	3.176	6.313	.5229	.66738	50.5922	3.1760	6.3130	.5228	.66750
20	10	22.5918	4.715	17.279	.3063	.92685	22.5574	4.7150	17.2793	.3062	.92685
40	10	44.3122	6.562	58.909	.6257	.72341	44.1521	6.5620	58.9081	.6257	.72341
5	20	6.1236	2.872	5.153	.0695	.99490	6.1341	2.8720	5.1535	.0695	.99498
20	20	21.6548	6.963	66.304	.3210	.93093	21.6401	6.9630	66.3042	.3209	.93093
40	20	21.0670	10.443	148.215	.3308	.93379	42.3611	10.8570	232.4673	.6566	.74067
5	30	5.7549	3.950	10.462	.0749	.99528	5.7531	3.9500	10.4616	.0749	.99528
20	30	21.0670	10.443	148.215	.3308	.93379	21.0470	10.4430	148.2161	.3308	.93379
40	30	41.7781	14.485	521.684	.6676	.74715	41.7331	14.4850	521.6839	.6675	.74714
5	40	5.6050	4.767	17.885	.0772	.99543	5.6018	4.7670	17.8857	.0772	.99542
20	40	20.9800	11.310	262.765	.3323	.93424	20.9720	11.3100	262.7653	.3322	.93424
40	40	41.5750	16.232	926.646	.6710	.74920	41.5406	16.2320	926.6473	.6710	.74920

TABLE 5 (cont)

Configuration		Properties from Tables					Properties Calculated from Correlations				
η_c deg	M_∞ W_∞/a_∞	η_s deg	Rho_s ρ_s/ρ_∞	P_s p_s/p_∞	θ_s rad	V_s W_s/W_∞	η_s deg	Rho_s ρ_s/ρ_∞	P_s p_s/p_∞	θ_s rad	V_s W_s/W_∞
ALTITUDE = 172,500 FEET											
22.5	3	31.9939	2.015	2.782	.2578	.88783	32.8968	2.0150	2.7816	.2577	.88793
30	3	31.9939	2.551	4.133	.3786	.80850	40.4257	2.5510	4.1336	.3786	.80858
40	3	51.6757	3.176	6.313	.5229	.66737	51.8459	3.1760	6.3131	.5228	.66749
20	10	22.5921	4.714	17.279	.3063	.92684	22.5585	4.1740	17.2788	.3062	.92686
40	10	44.2764	6.608	58.906	.6263	.72372	45.2110	6.6080	58.9064	.6262	.72373
50	10	55.1490	8.050	83.571	.7860	.58045	56.1392	8.0500	83.5710	.7859	.58046
5	20	6.1236	2.872	5.153	.0695	.99499	6.1341	2.8720	5.1535	.0695	.99498
20	20	21.6325	7.048	66.308	.3214	.93104	21.6171	7.0480	66.3080	.3213	.93103
40	20	42.4818	11.046	232.463	.6574	.74111	42.3158	11.0460	232.4637	.6573	.74111
5	30	5.755	3.950	10.462	.0749	.99528	5.7531	3.9500	10.4619	.0749	.99528
20	30	21.0457	10.643	148.224	.3312	.93390	21.0253	10.6430	148.2243	.3311	.93390
40	30	41.7306	14.855	521.678	.6684	.74763	41.733	14.8550	521.6775	.6683	.74762
5	50	5.6050	4.766	17.885	.0772	.99543	5.6018	4.7660	17.8847	.0772	.99542
20	40	20.9613	11.516	262.774	.3326	.93434	20.9554	11.5160	262.7732	.3325	.93433
40	40	41.5346	16.633	926.639	.6717	.74962	41.5011	16.6330	926.6386	.6717	.74961

TABLE 5 (cont)

Configuration		Properties from Tables					Properties Calculated from Correlations				
η_c deg	M_∞ W_∞/a_∞	η_s deg	Rho_s ρ_s/ρ_∞	P_s p_s/p_∞	θ_s rad	V_s W_s/W_∞	η_s deg	Rho_s ρ_s/ρ_∞	P_s p_s/p_∞	θ_s rad	V_s W_s/W_∞
ALTITUDE = 200,000 FEET											
22.5	3	31.9988	2.015	2.782	.5778	.88581	32.0146	2.0150	2.7821	.2577	.88789
30	3	39.7710	2.015	4.133	.3785	.80845	39.4602	2.5490	4.1335	.3785	.80854
40	3	51.7081	3.171	6.314	.5225	.66714	50.6157	3.1710	5.1260	.5224	.97991
20	10	22.6100	4.687	17.278	.3060	.92677	22.5763	4.6870	17.2779	.3059	.92678
40	10	44.3384	6.528	58.908	.6253	.72318	44.1808	6.5280	58.9081	.6252	.72319
5	20	6.1253	2.869	5.153	.0695	.99498	6.1364	2.8690	5.1535	.0695	.99498
20	20	21.6587	6.947	66.301	.3209	.93091	21.6441	6.9470	66.3014	.3209	.93091
40	20	42.3783	11.087	232.465	.6575	.74121	42.3049	11.0870	232.4648	.6575	.74120
5	30	5.7584	3.935	10.461	.0749	.99528	5.7571	3.9350	10.4608	.0748	.99528
20	30	21.0424	10.673	148.223	.3312	.93392	21.0224	10.6730	148.2232	.3312	.93392
40	30	41.7011	15.094	521.672	.6689	.74792	41.6558	15.0940	521.6708	.6688	.74792
5	40	5.6092	4.738	17.884	.0772	.99542	5.6064	4.7380	17.8834	.0771	.99542
20	40	20.9532	11.609	262.78	.3327	.93438	20.9473	11.6090	262.7795	.3327	.93438
40	40	41.4656	17.369	926.623	.6729	.75032	41.4317	17.3690	926.6244	.6728	.75032

TABLE 6

Comparison of shock angle correlations

$M_\infty \sin \eta_s = A_0 + A_1 K_C$ for $6 \leqslant K_C \leqslant 25$

Altitude (ft)	Pressure (atm)	Hudgins		Romig	
		A_0	A_1	A_0	A_1
0	1.0	0.3446	1.0303	0.390	1.030
36,100	0.2239	0.4022	1.0278	1.3925	1.0267
65,000	0.0538	0.4326	1.0231	1.4027	1.0237
100,000	0.1100	0.4426	1.0197	0.4096	1.0202
125,000	0.00367	0.4293	1.0175	0.4144	1.0178
155,500	0.00109	0.4094	1.0158	0.4199	1.0150
200,000	0.00195	0.4287	1.0128	0.4279	1.0110

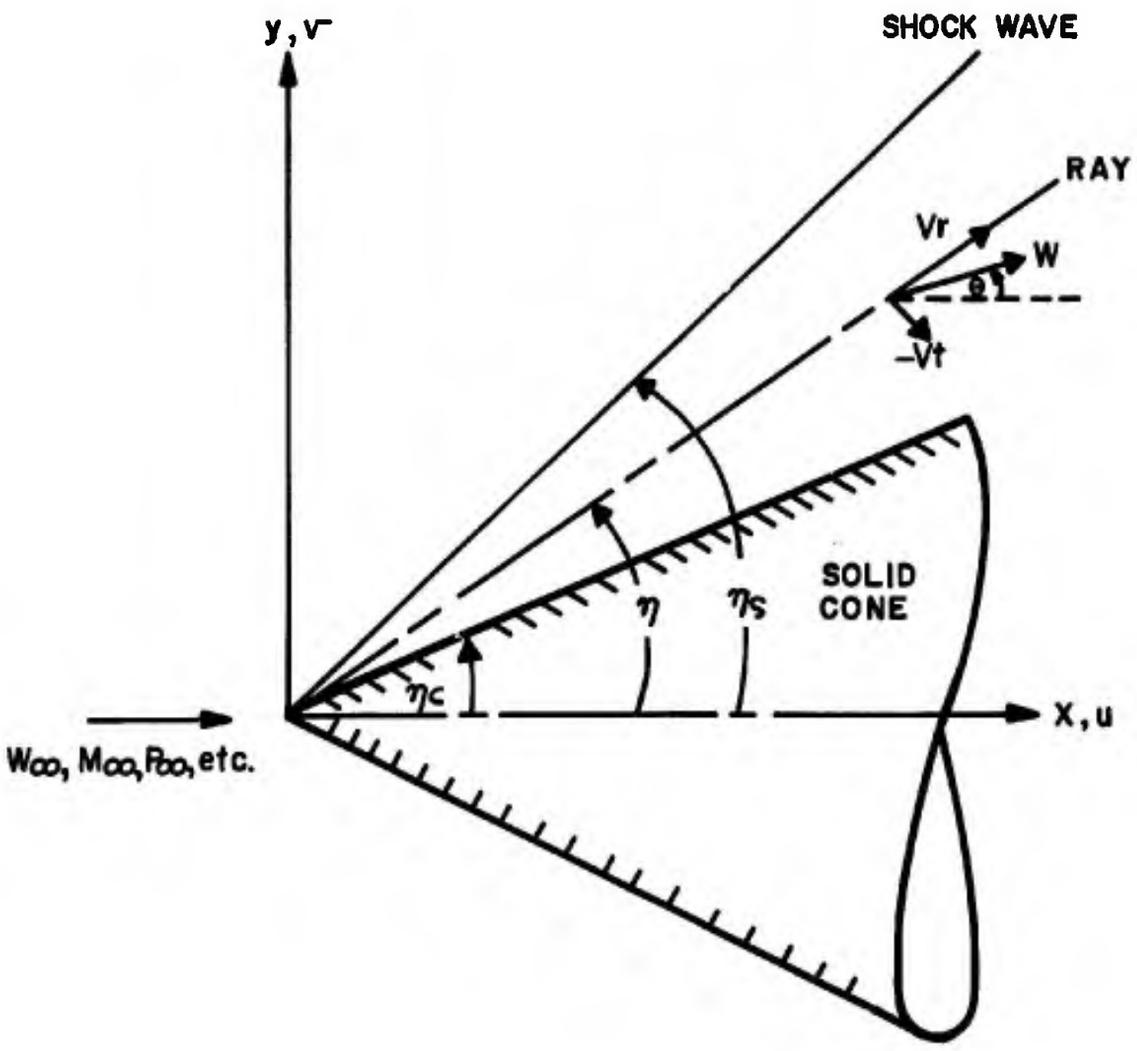

Fig 1 Geometry of conical flow

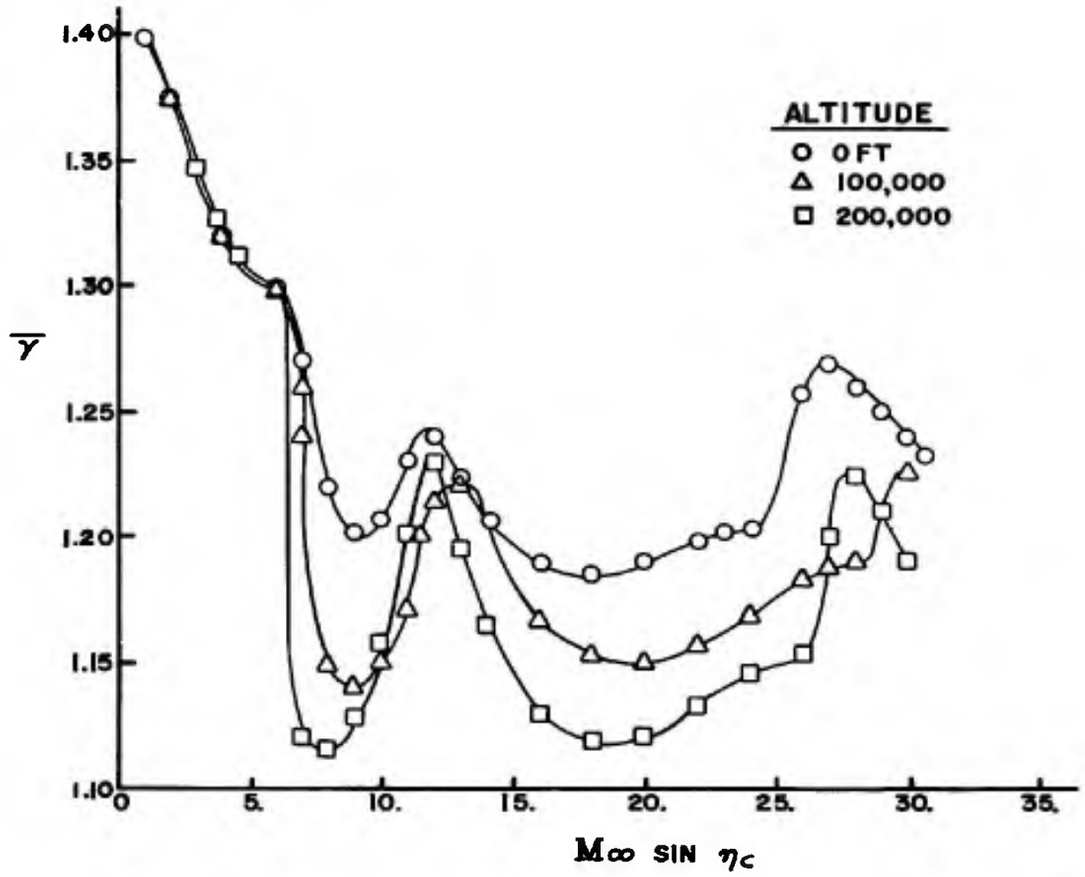

Fig 2 Average gamma versus hypersonic similarity parameter

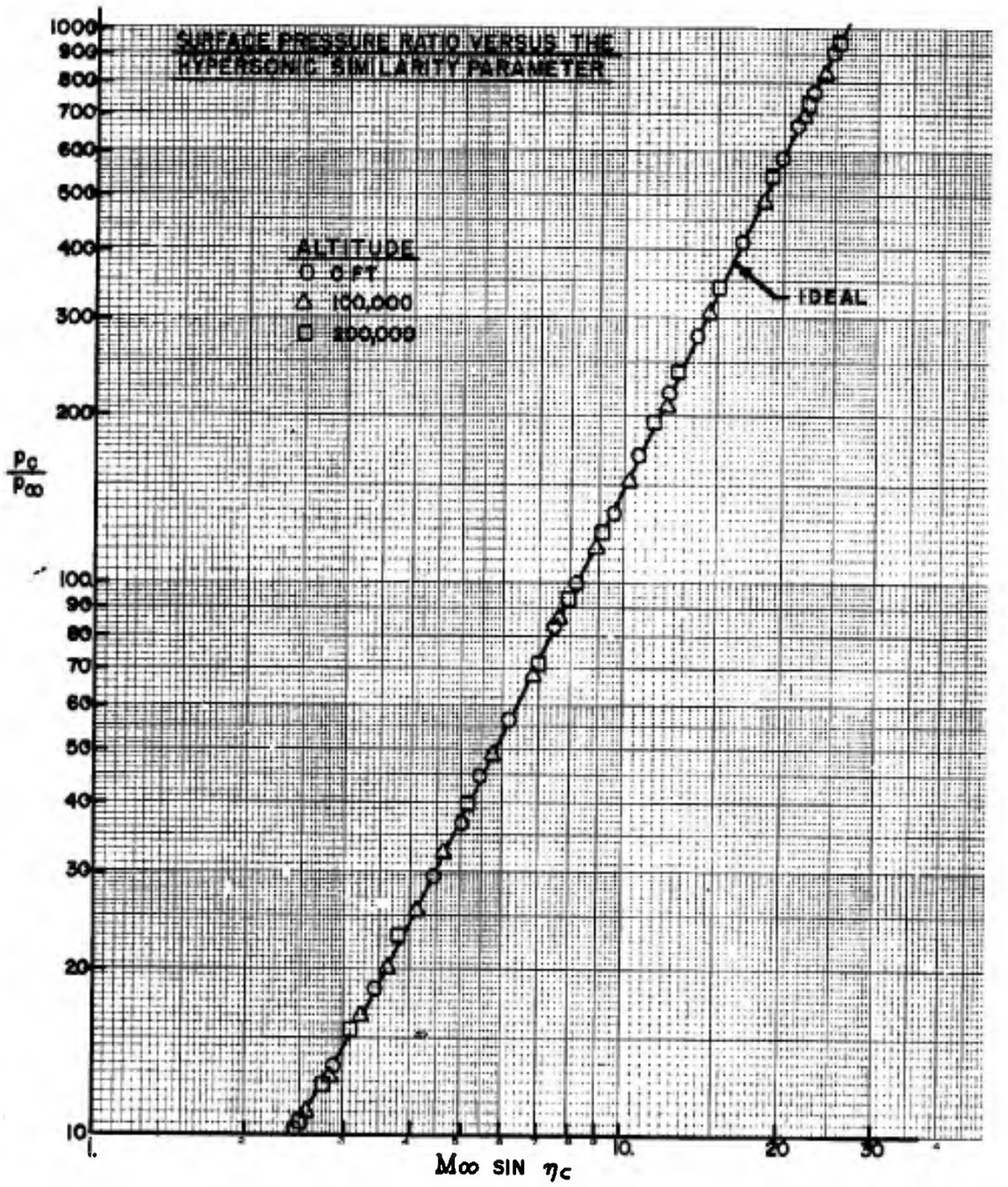

Fig 3 Surface pressure ratio versus the hypersonic similarity parameter

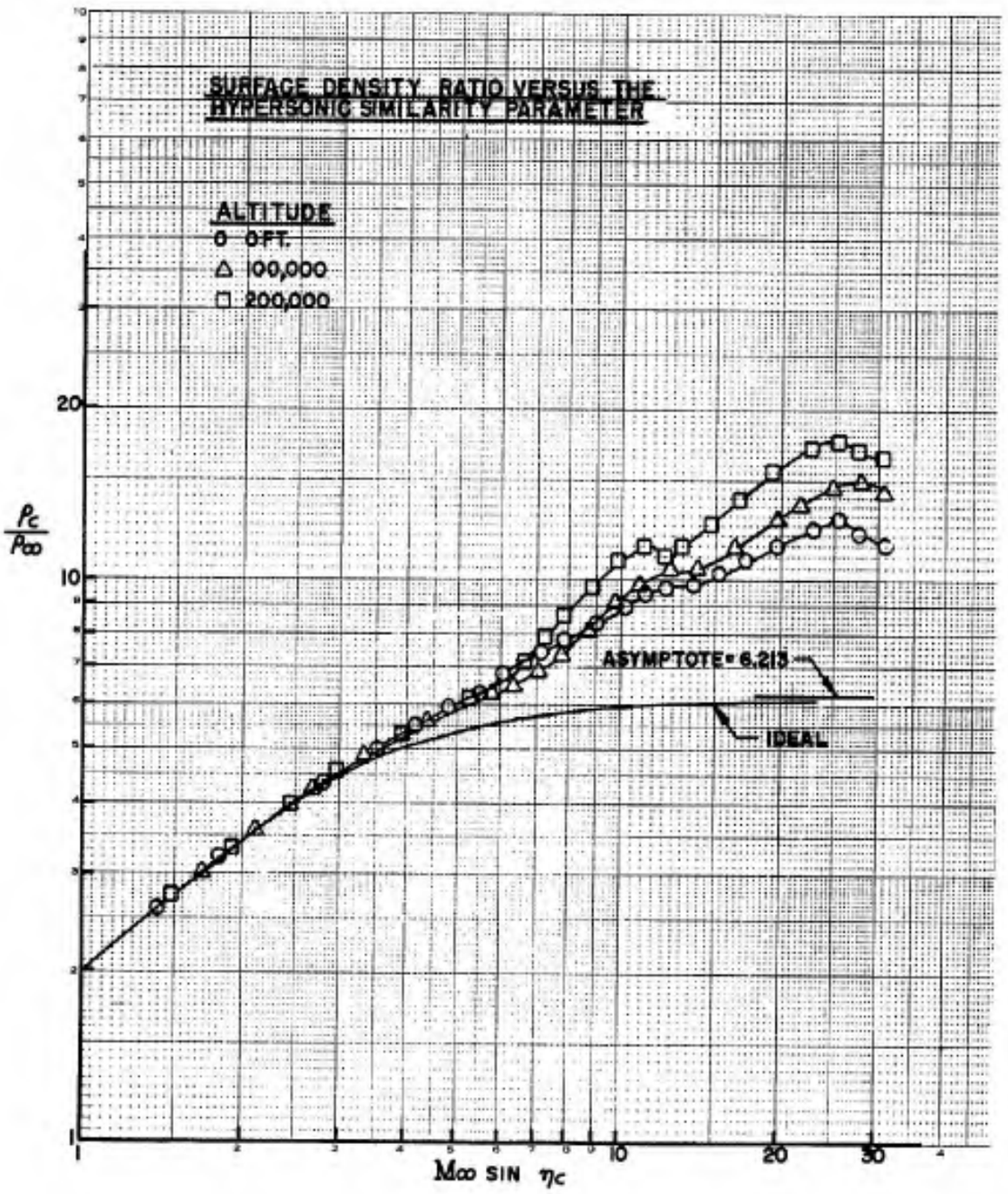

Fig 4 Surface density ratio versus the hypersonic similarity parameter

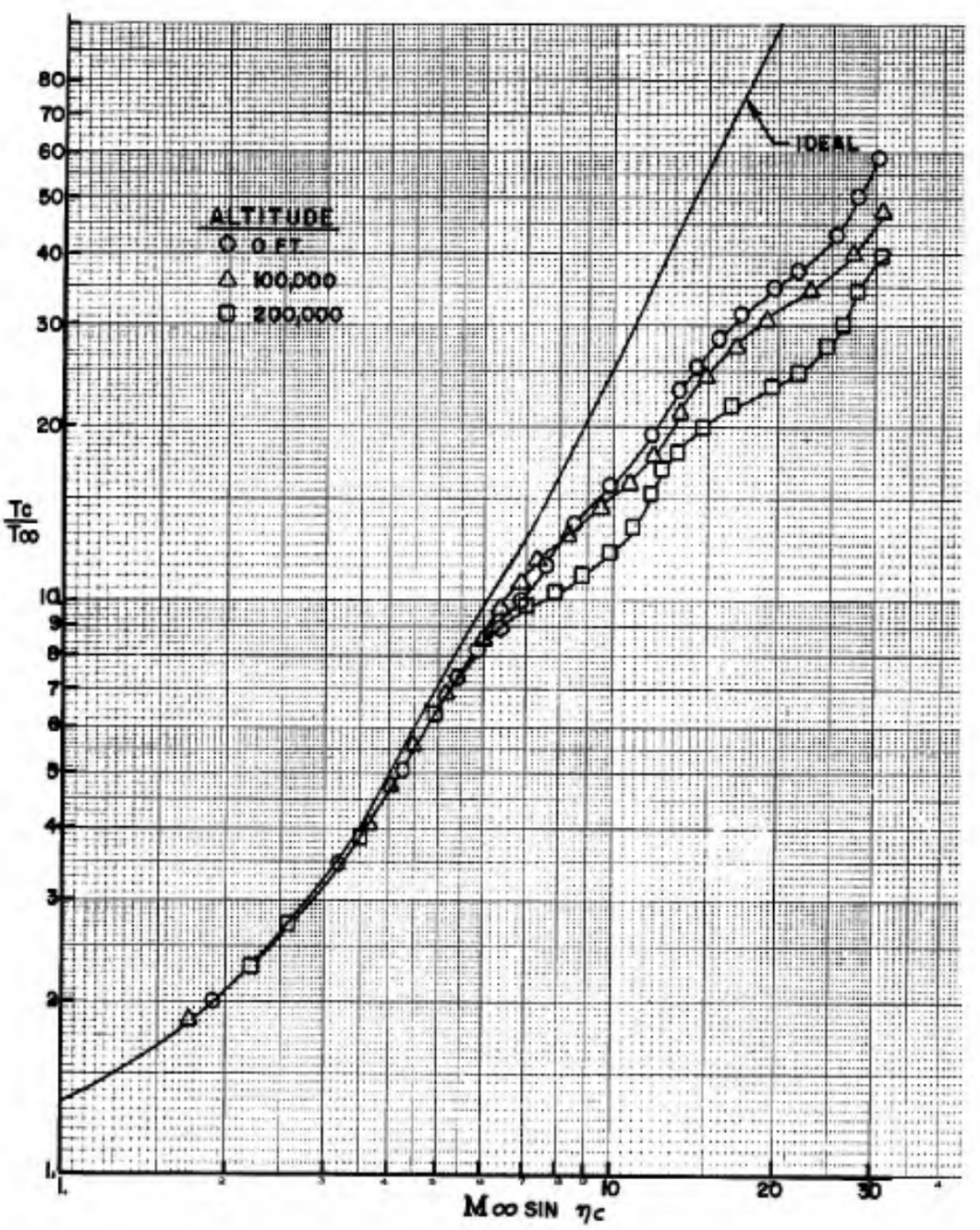

Fig 5 Surface temperature ratio versus the hypersonic similarity parameter

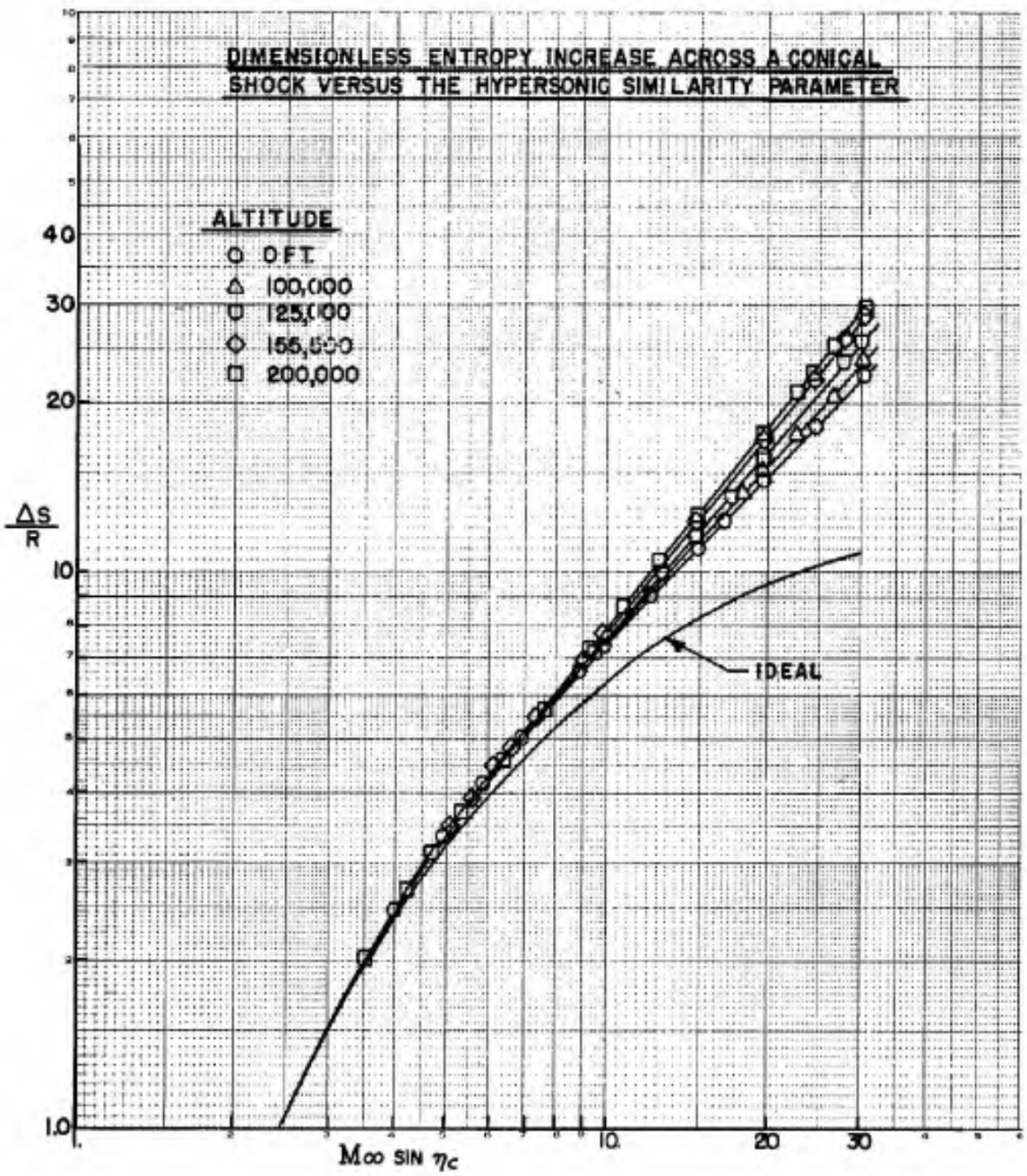

Fig 6 Dimensionless entropy increase across a conical shock versus the hypersonic similarity parameter

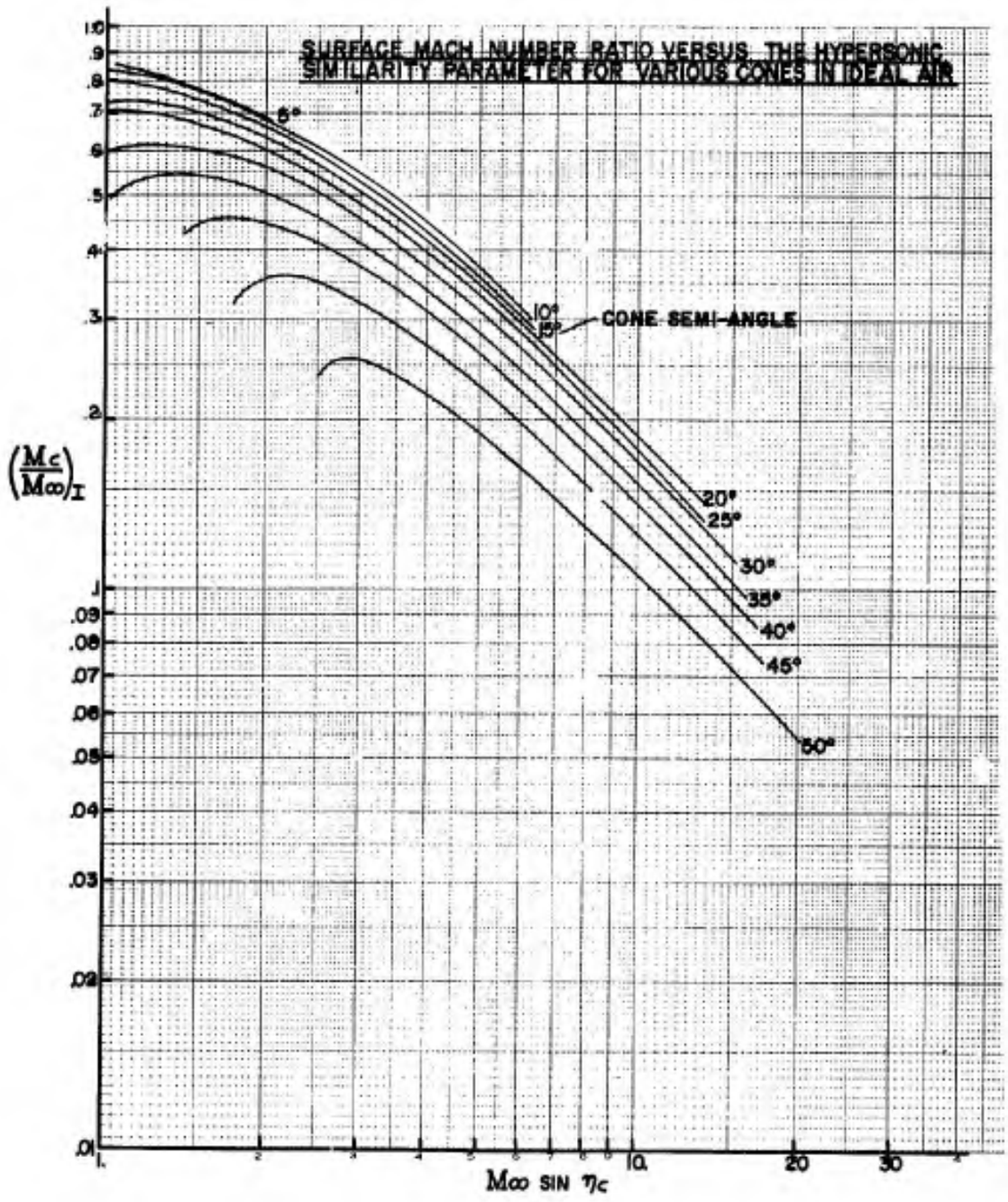

Fig 7A Surface Mach number ratio versus the hypersonic similarity parameter for various cones in ideal air

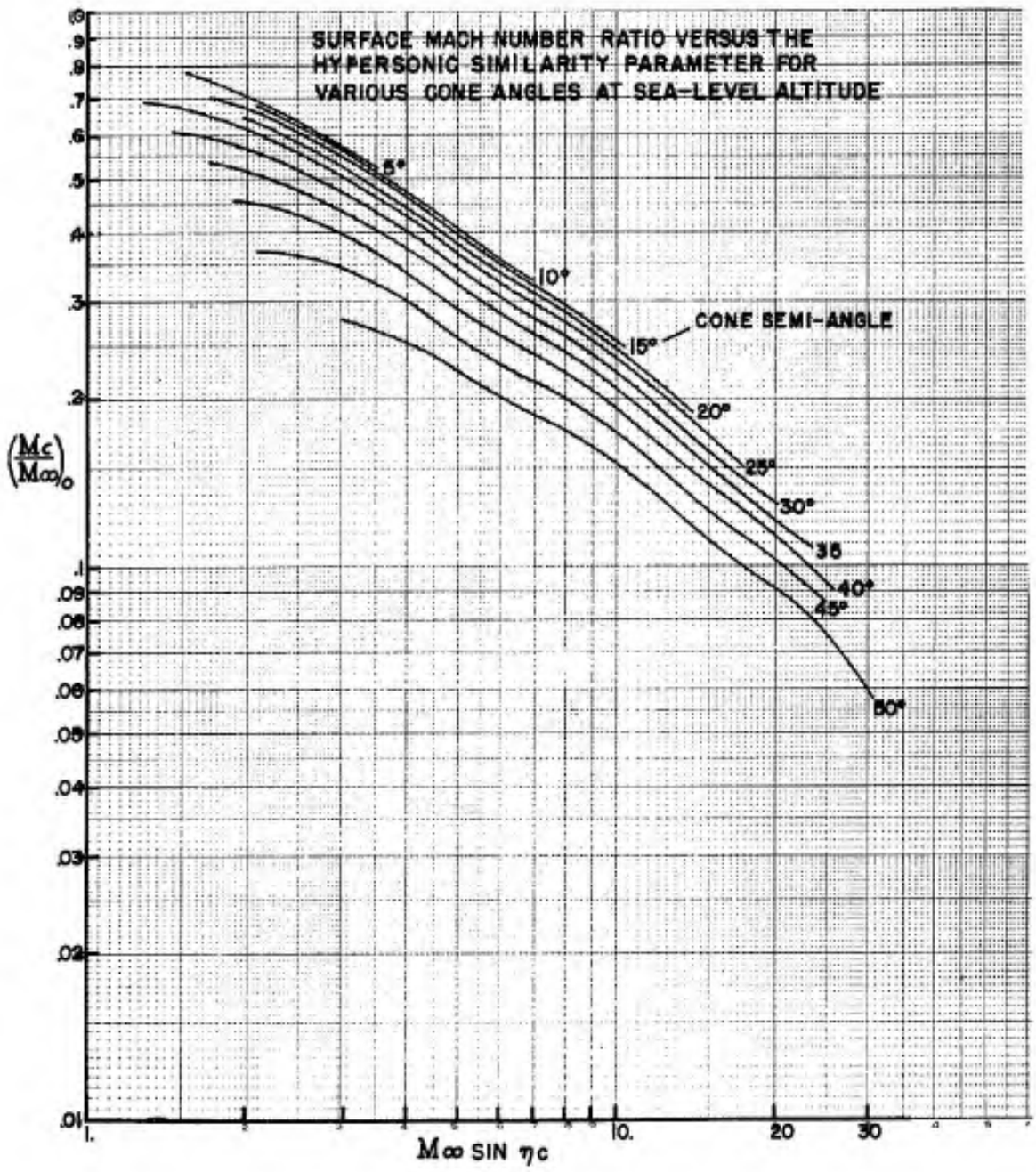

Fig 7B Surface Mach number ratio versus the hypersonic similarity parameter tor various cone angles at sea-level altitude

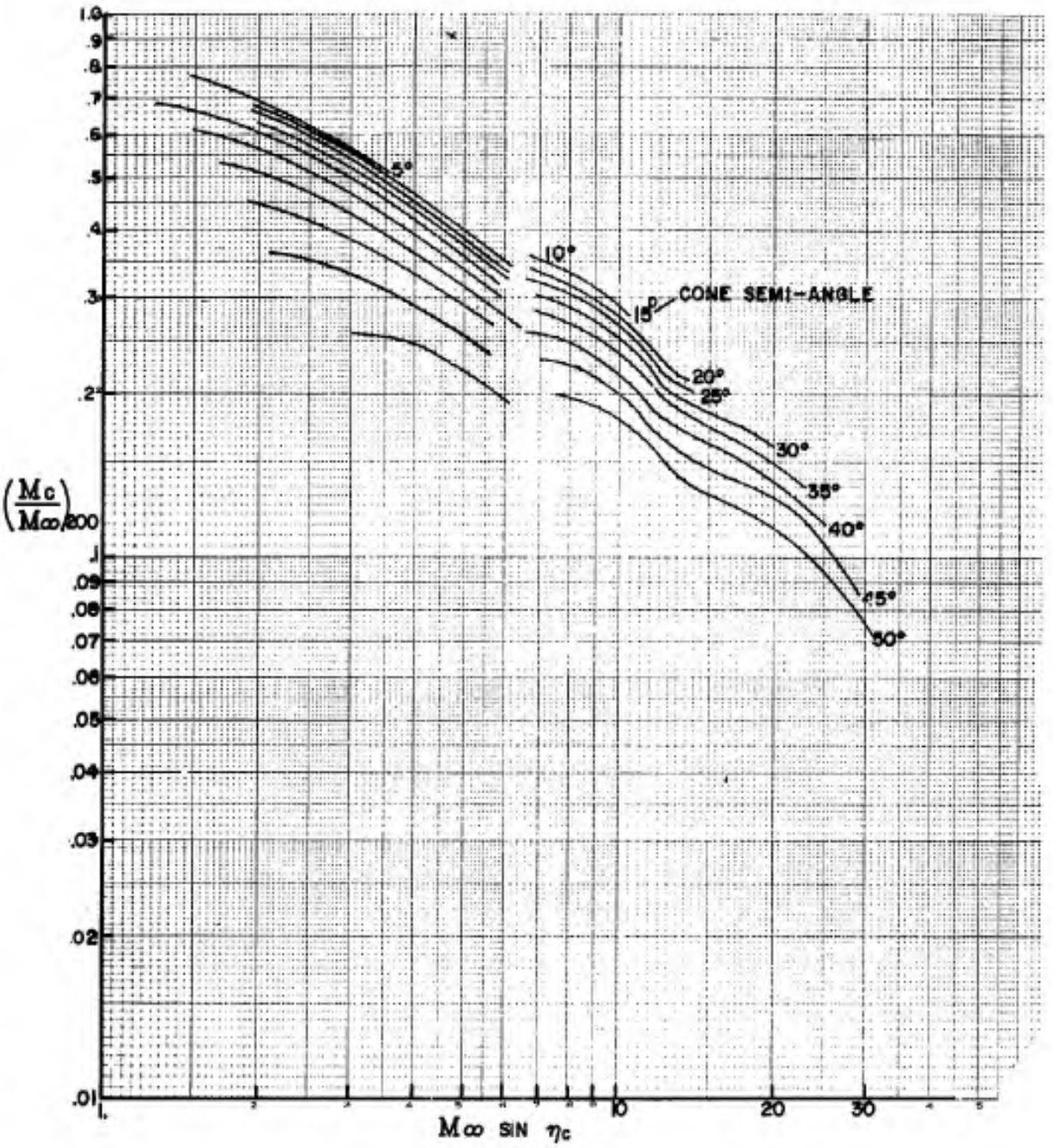

Fig 7C Surface Mach number ratio versus the hypersonic similarity parameter for various cone angles at 200,000 feet altitude

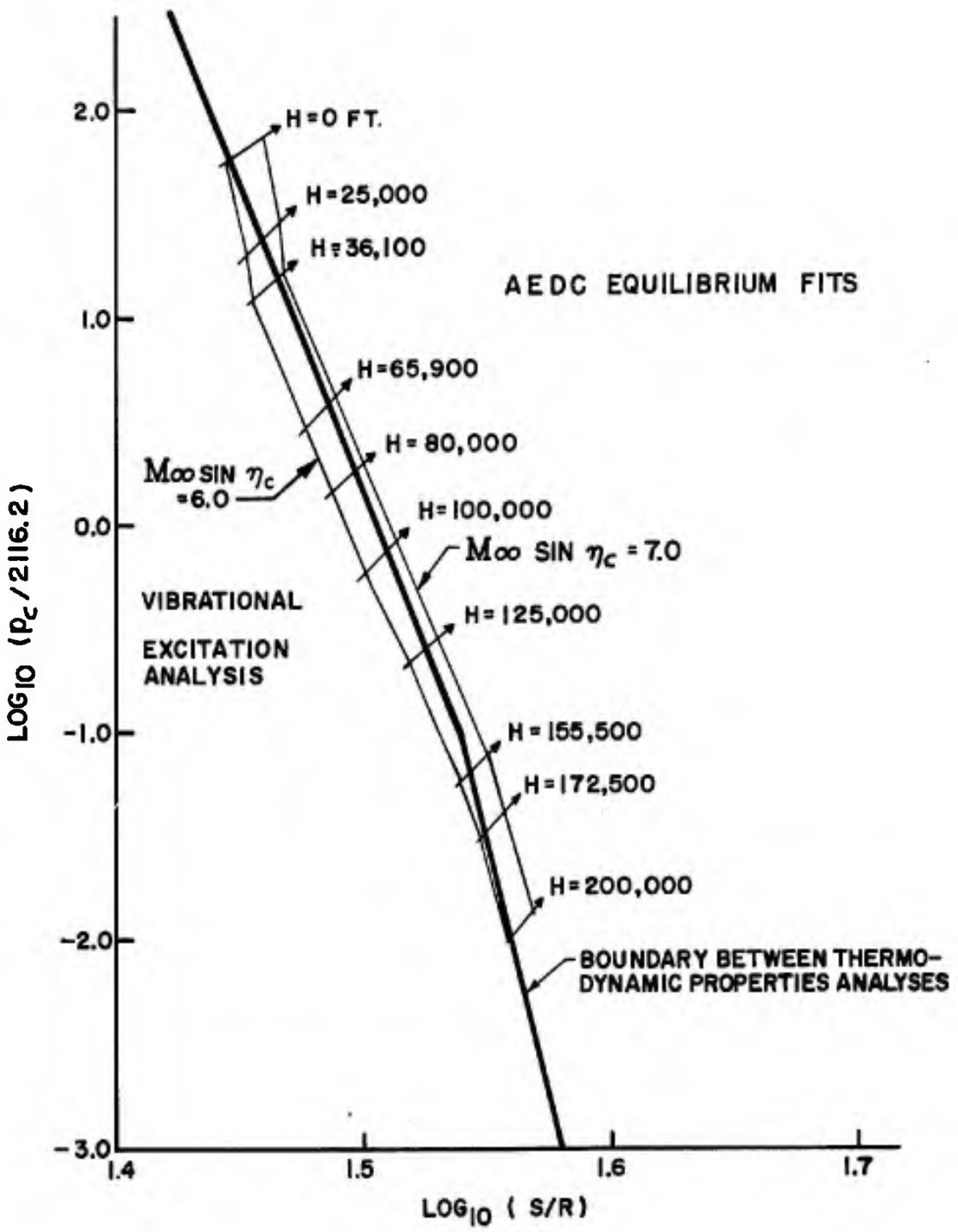

Fig 8 Crossing of thermodynamic properties analyses boundary as a function of $M_\infty \sin \eta_c$ and altitude

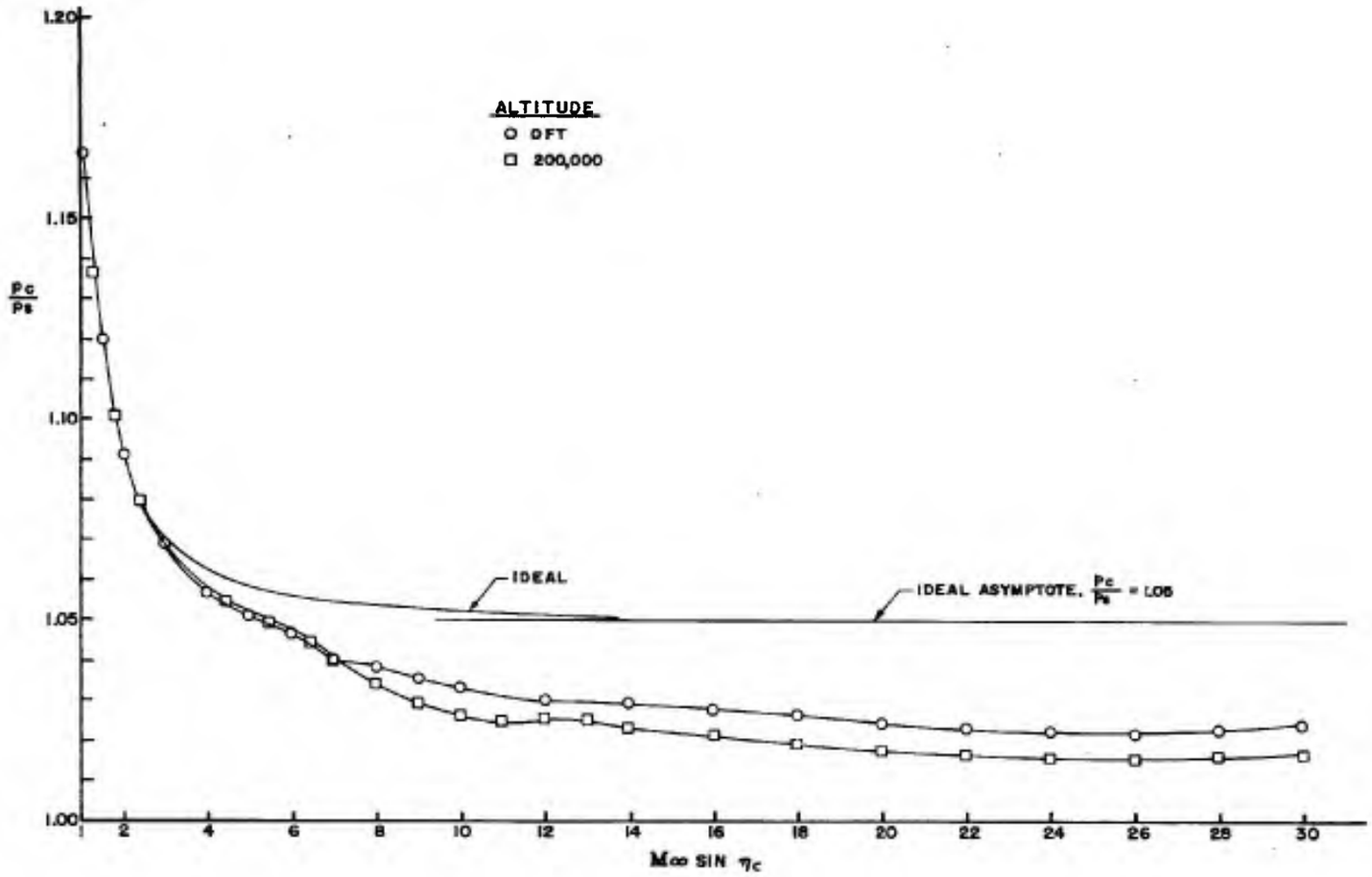

Fig 9 Ratio of surface to shock pressure versus the hypersonic similarity parameter

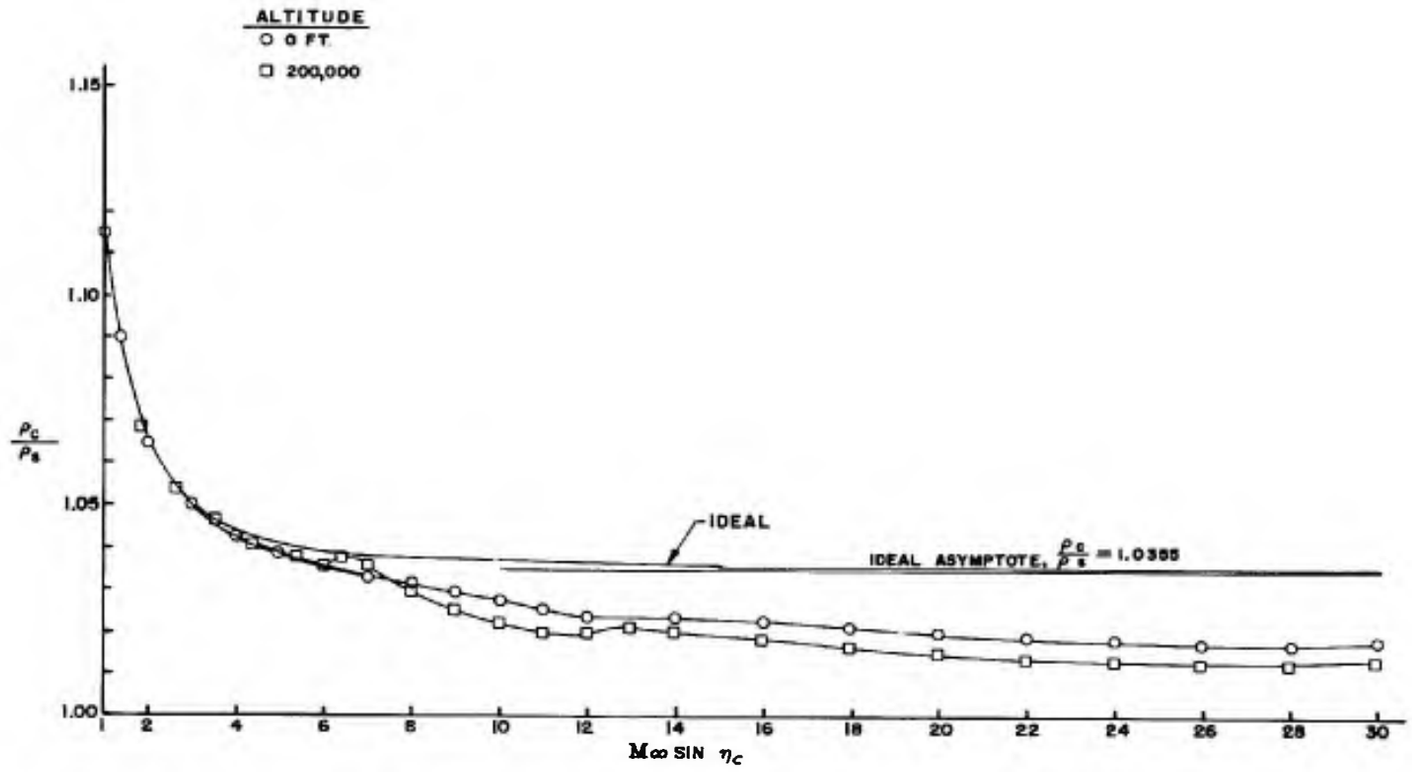

Fig 10 Ratio of surface to shock density versus the hypersonic similarity parameters

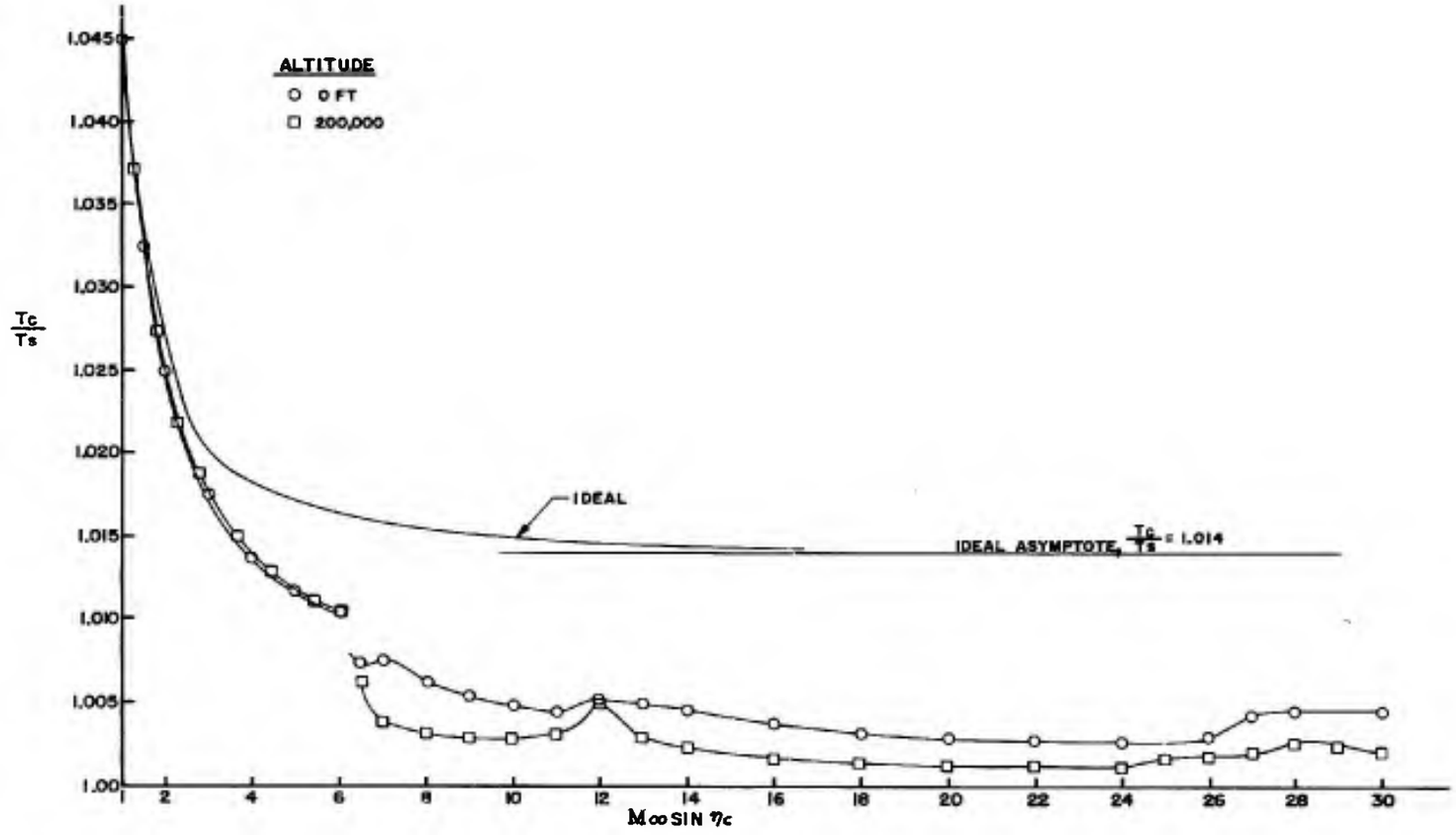

Fig 11 Ratio of surface to shock temperature versus the hypersonic similarity parameter

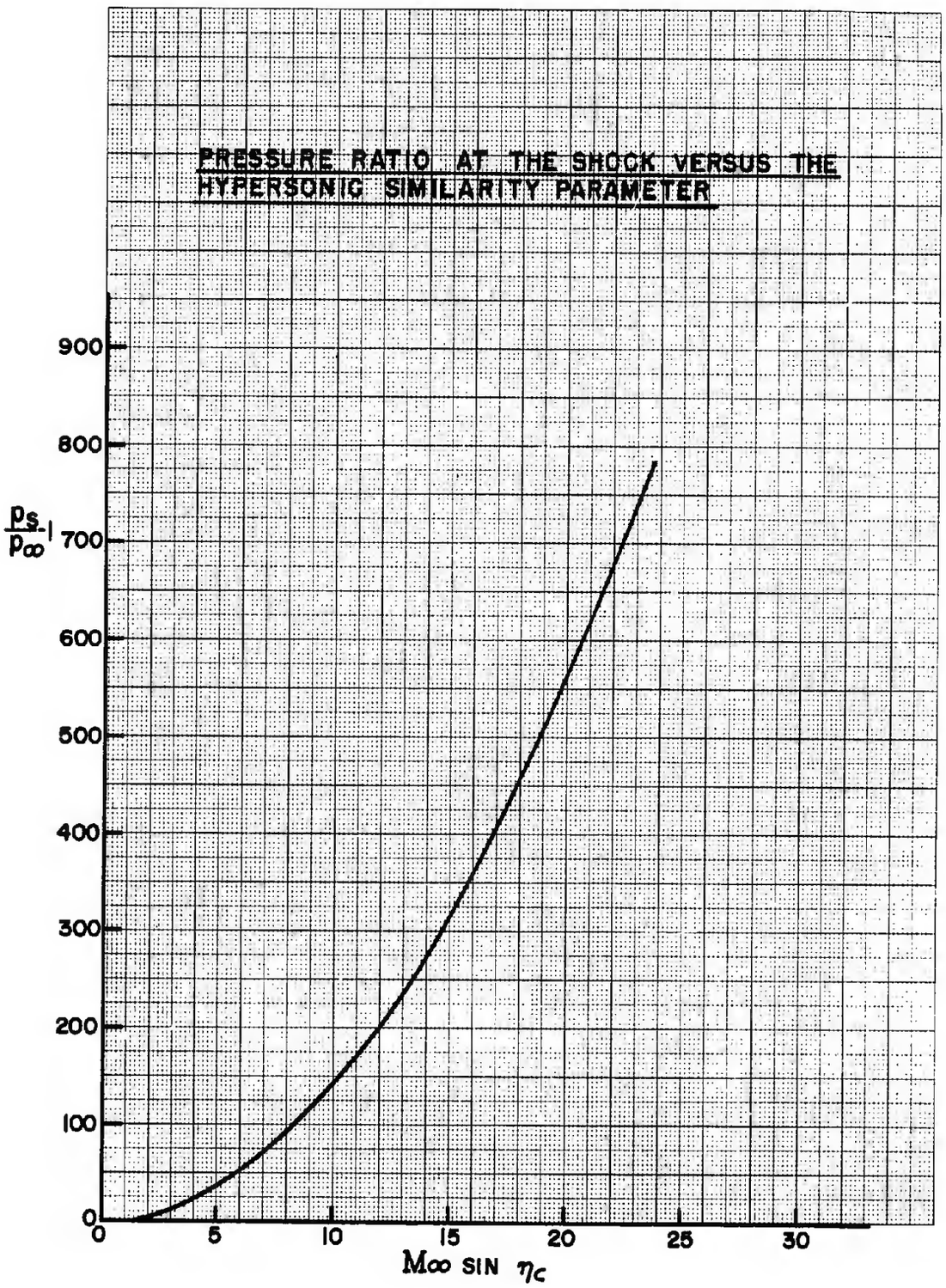

Fig 12 Pressure ratio at the shock versus the hypersonic similarity parameter

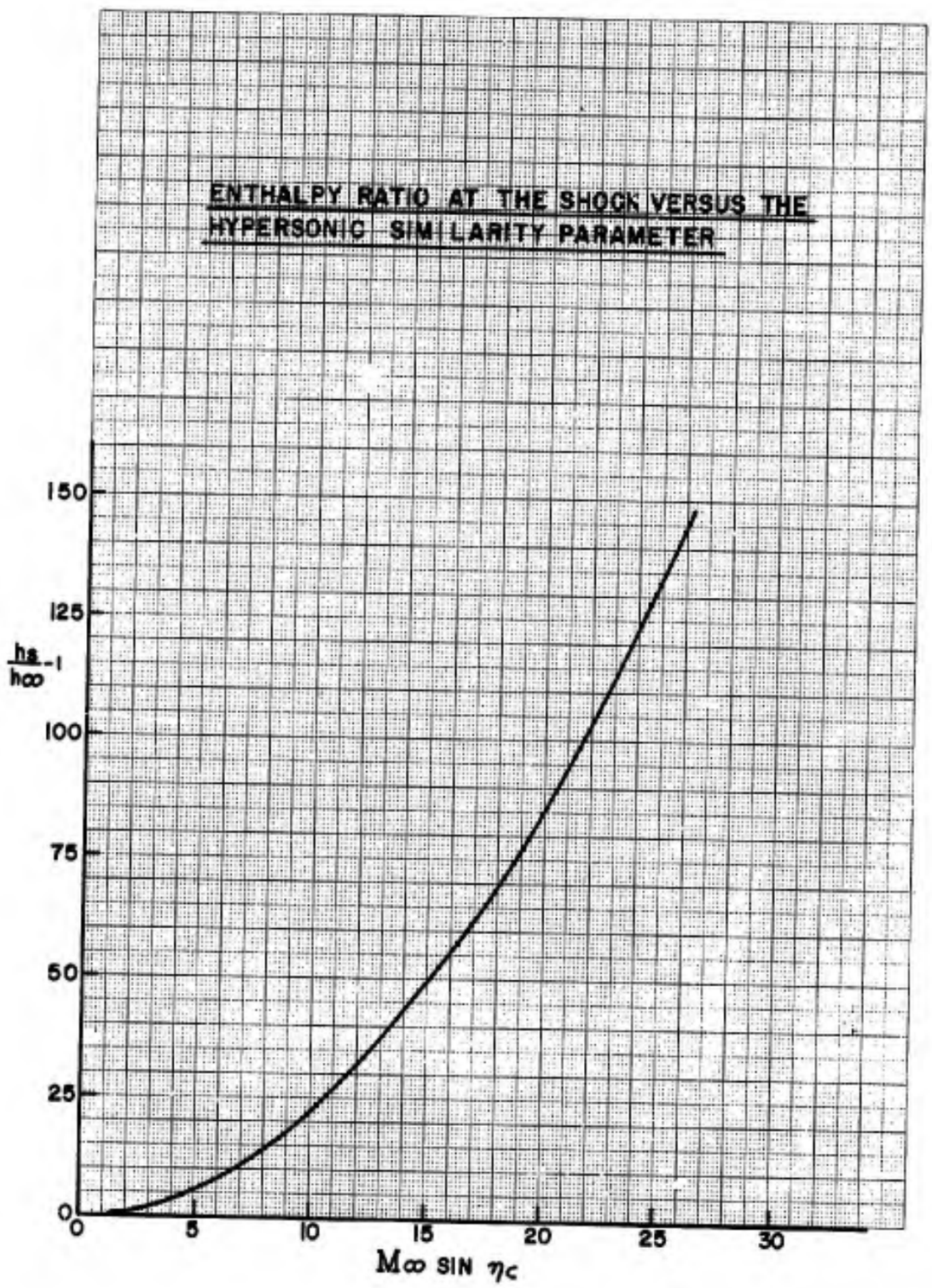

Fig 13 Enthalpy ratio at the shock versus the hypersonic similarity parameter

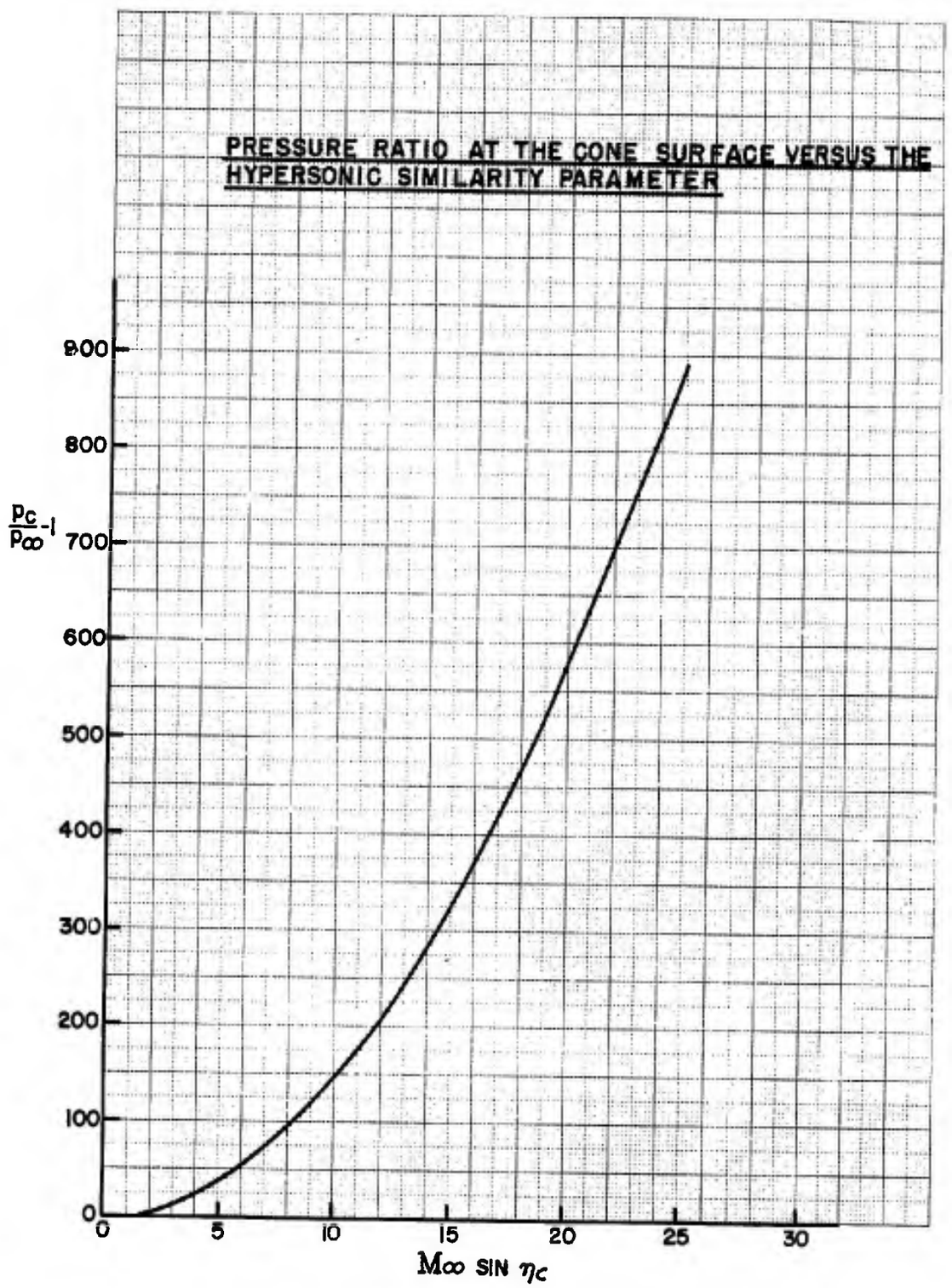

Fig 14 Pressure ratio at the cone surface versus the hypersonic similarity pcrameter

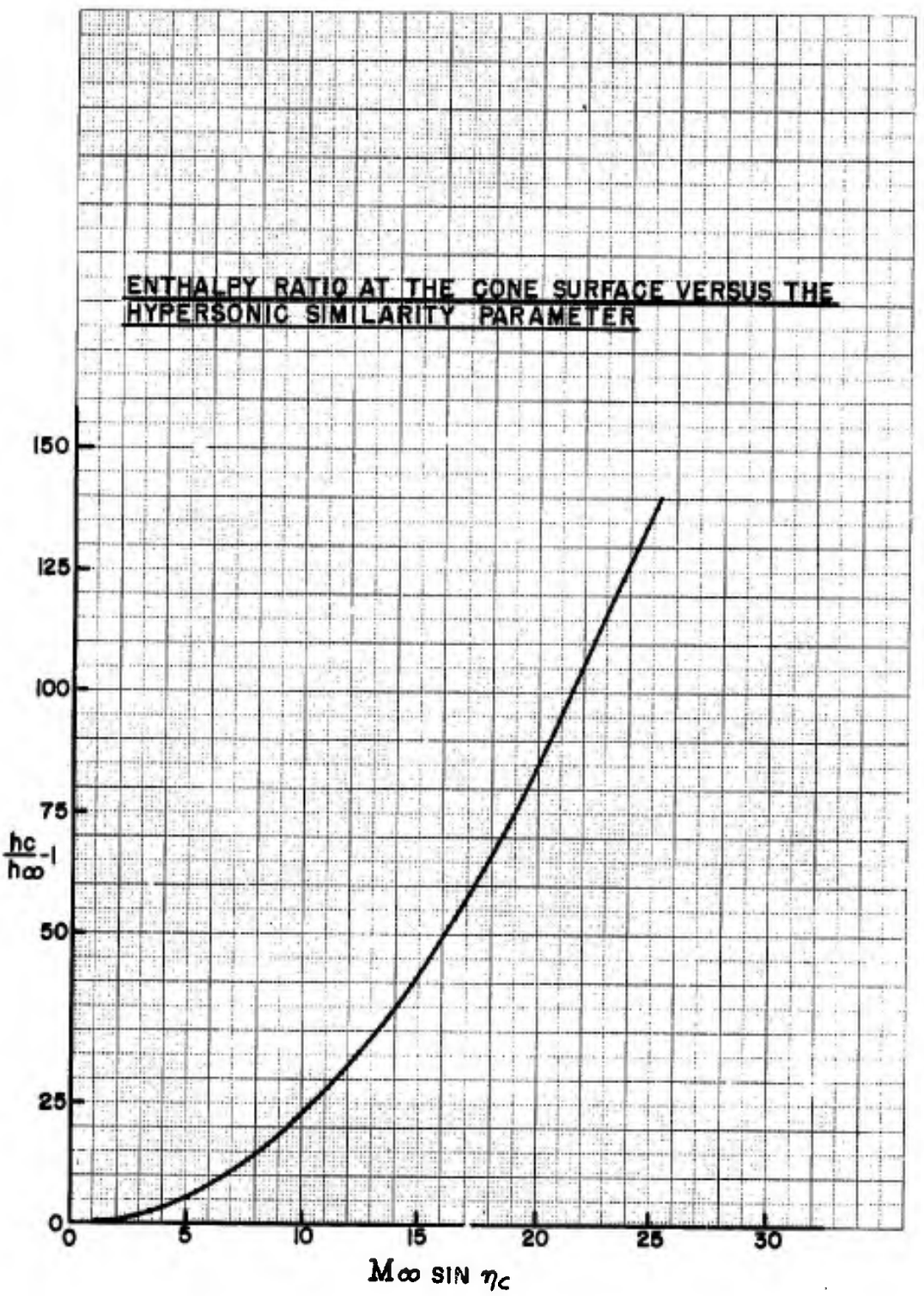

Fig 15 Enthalpy ratio at the cone surface versus the hypersonic similarity parameter

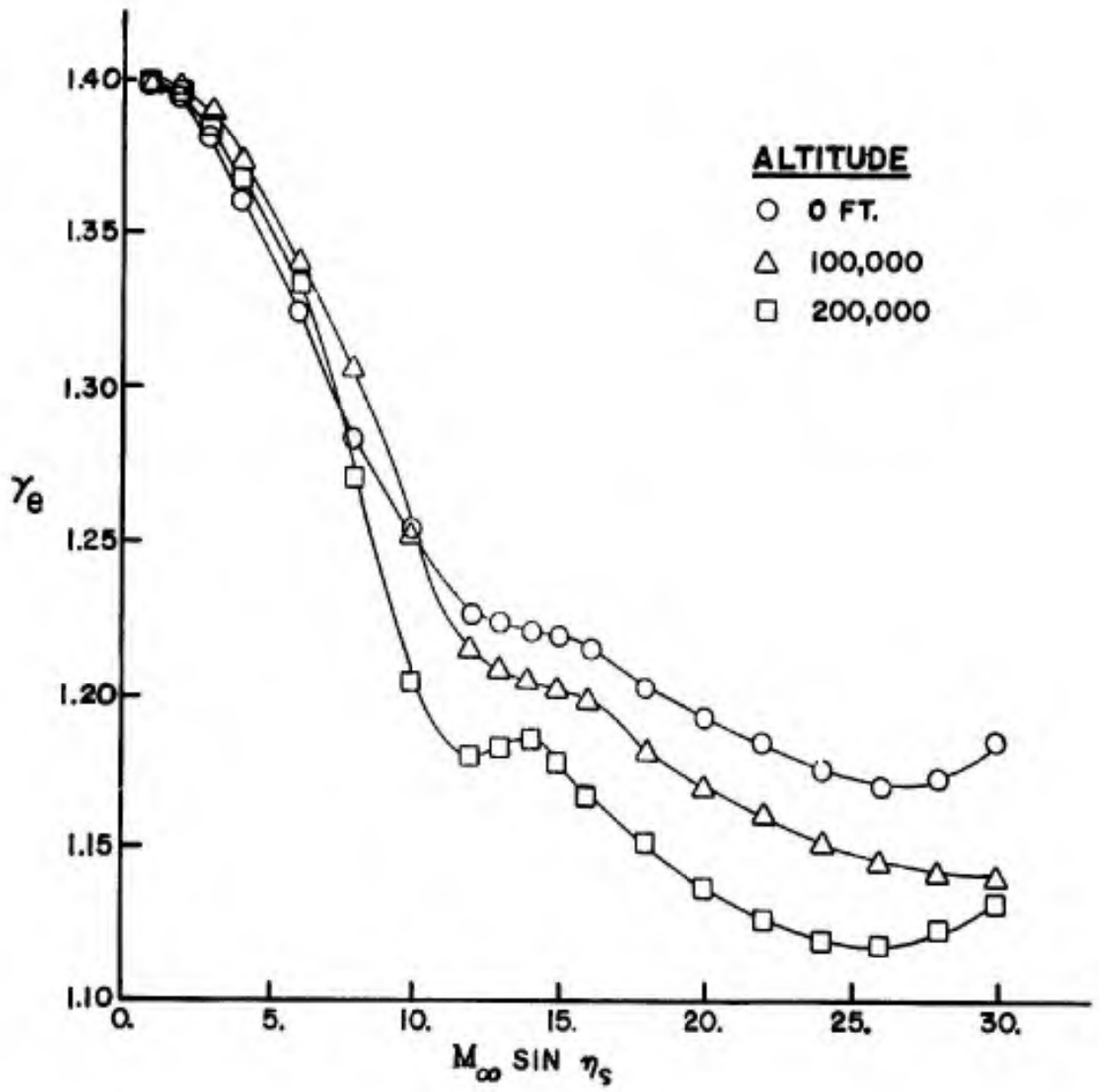

Fig 16 Effective gamma versus M_∞ sin η_s

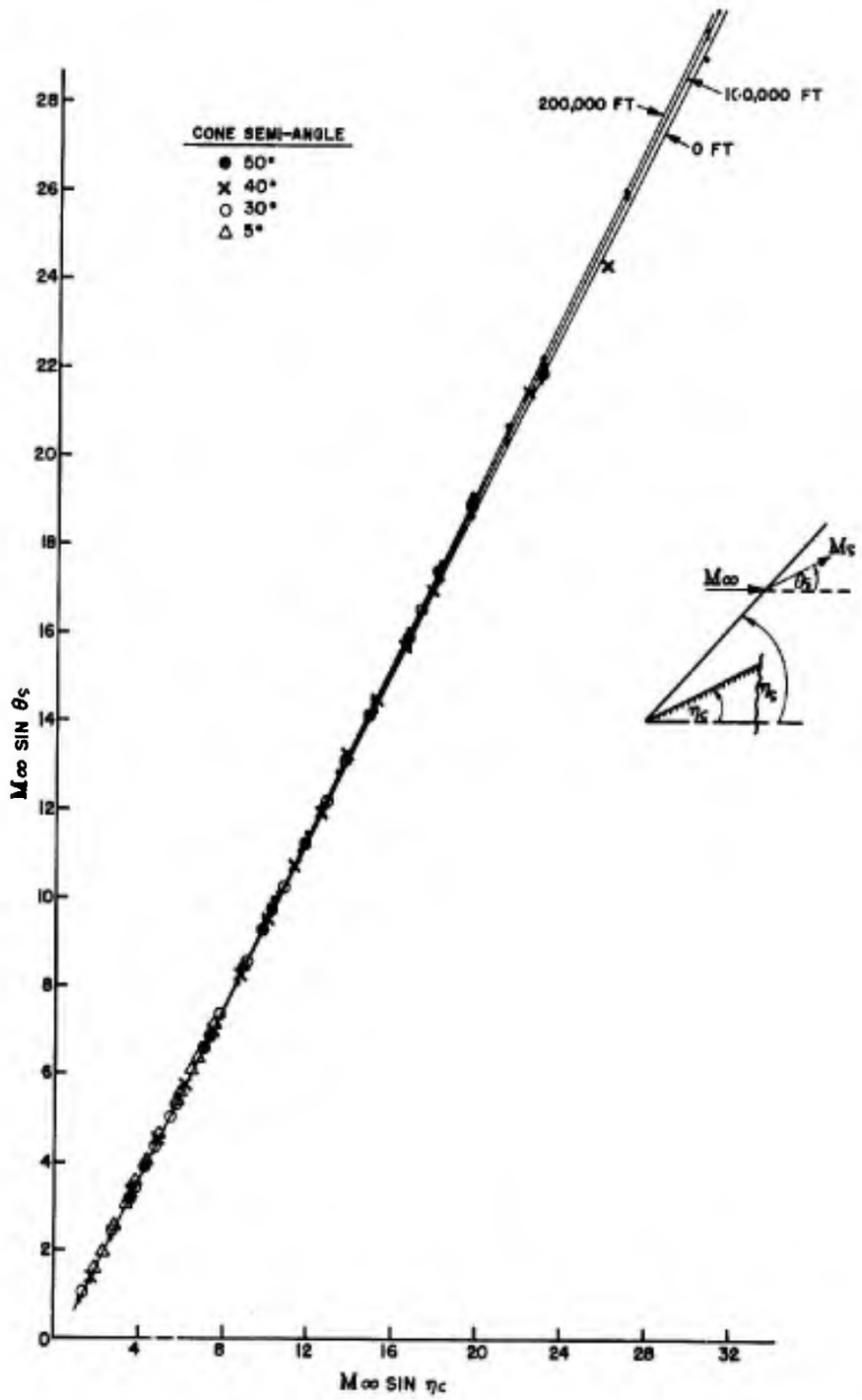

Fig 17 Correlation of flow deflection angle with Mach number and cone angle

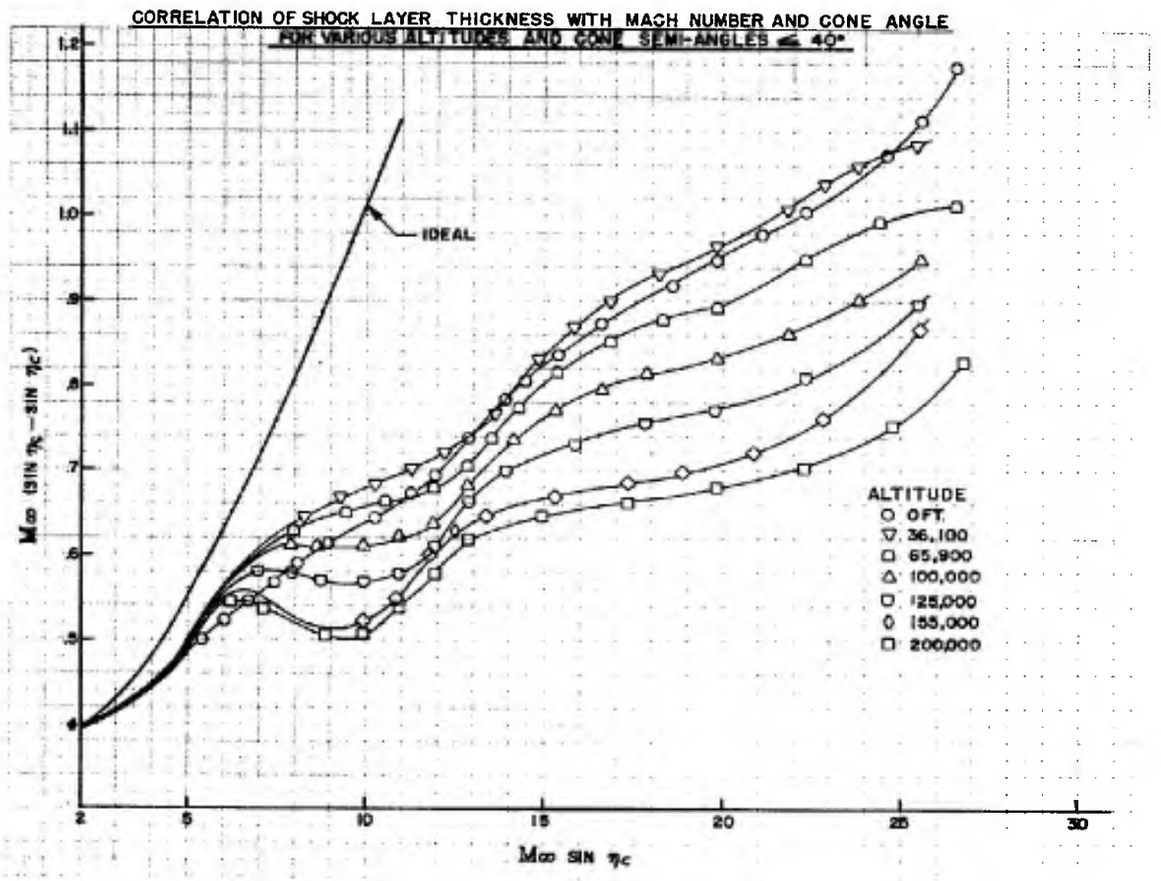

Fig 18 Correlation of shock layer thickness with Mach number and cone angle for various altitudes and cone semi-angles $\leq 40°$

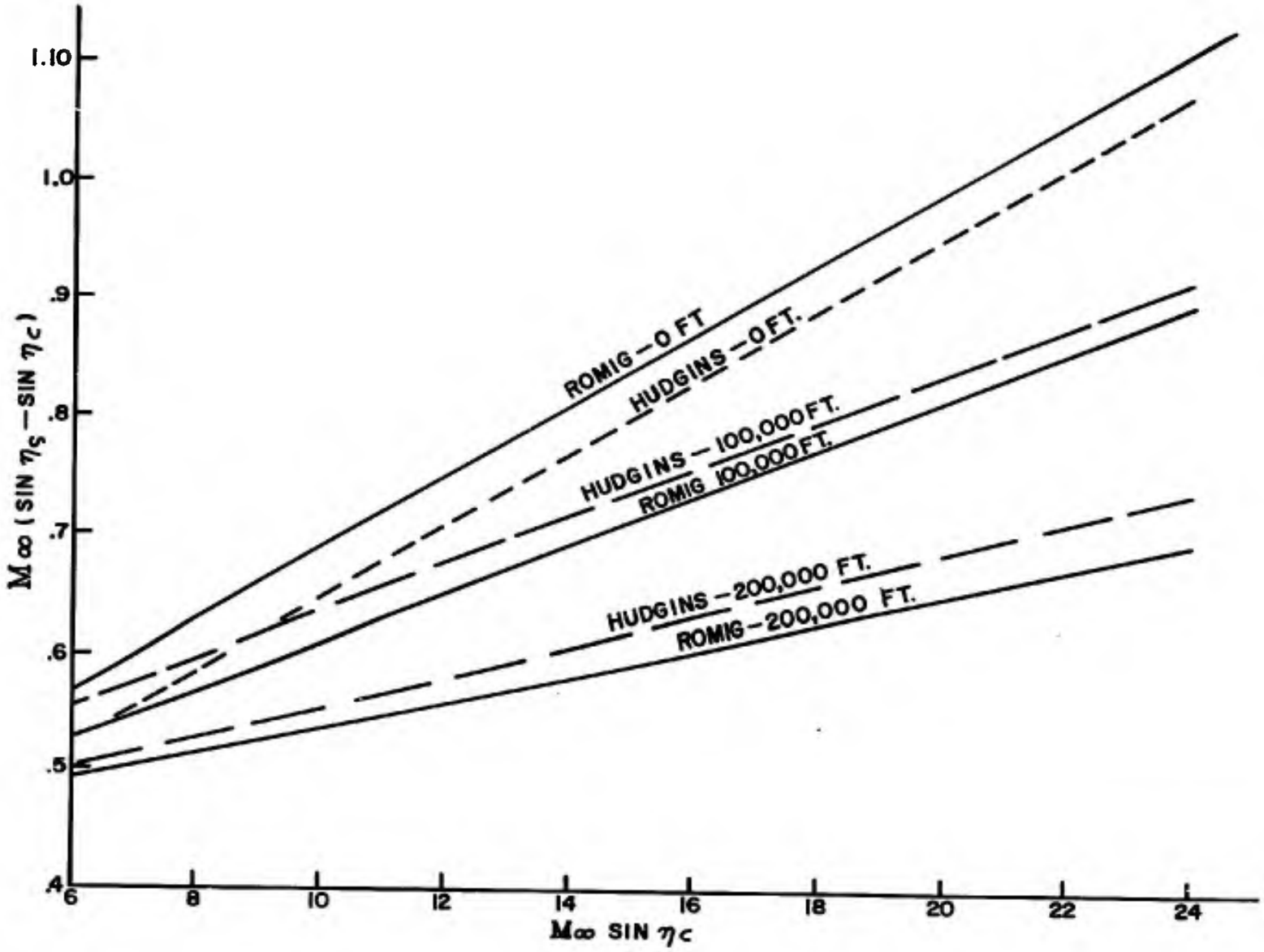

Fig 19 Comparison of shock layer thickness results

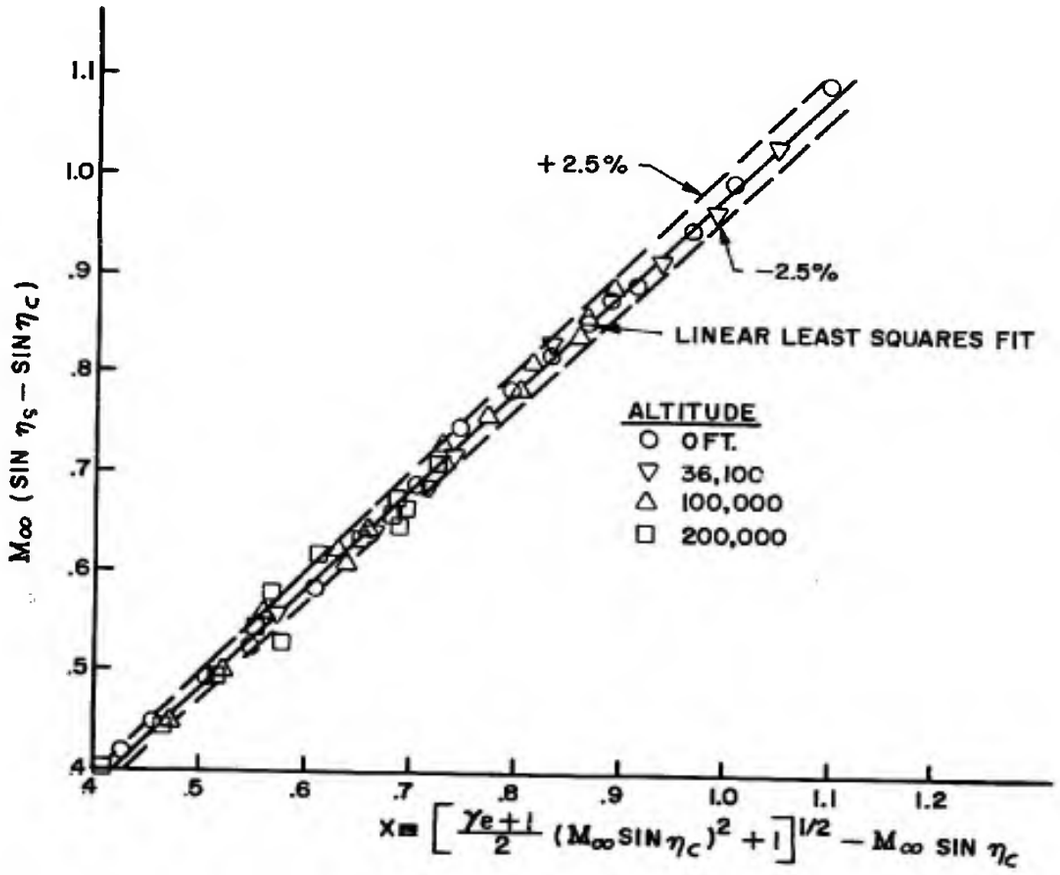

Fig 20 Correlation of shock layer thickness with Mach number, cone angle and effective gamma